NAUTICAL LABORATORY

CALIFORNIA INSTITUTE OF TECHNOLOGY

HYPERSONIC RESEARCH PROJECT

Memorandum No. 32

June 15, 1956

AN EXPERIMENTAL INVESTIGATION OF THE FLOW OVER BLUNT-NOSED CONES AT A MACH NUMBER OF 5.8

by

Reginald M. Machell

Lieutenant, U. S. Navy

and

William T. O' Bryant

Commander, U. S. Navy

ARMY ORDNANCE CONTRACT NO. DA-04-495-Ord-19

GUGGENHEIM AERONAUTICAL LABORATORY
CALIFORNIA INSTITUTE OF TECHNOLOGY
Pasadena, California

HYPERSONIC RESEARCH PROJECT

Memorandum No. 32

June 15, 1956

AN EXPERIMENTAL INVESTIGATION OF THE FLOW OVER BLUNT-NOSED CONES AT A MACH NUMBER OF 5.8

by

Reginald M. Machell
Lieutenant, U. S. Navy

and

William T. O'Bryant
Commander, U. S. Navy

Clark B. Millikan, Director
Guggenheim Aeronautical Laboratory

ARMY ORDNANCE CONTRACT NO. DA-04-495-Ord-19
Army Project No. 5B0306004
Ordnance Project No. TB3-0118
OOR Project No. 1600-PE

ACKNOWLEDGMENTS

The authors wish to express their appreciation to Professor Lester Lees for his interest and guidance during the course of this investigation. Helpful suggestions and criticisms were received from Mr. James M. Kendall, Mr. Robert E. Oliver, and Mr. Toshi Kubota, and their assistance is gratefully acknowledged. Sincere thanks are extended to the staff of the GALCIT hypersonic wind tunnel for their cooperation and assistance, to Mr. C. A. Bartsch and Mr. George Carlson of the GALCIT machine shop who skillfully constructed the models, to Mrs. Fae S. Kelley who performed many of the calculations and prepared the graphs, and to Mrs. H. Van Gieson who typed the final manuscript and supplied many helpful suggestions.

ABSTRACT

Shock shapes were observed and static pressures were measured on spherically-blunted cones at a nominal Mach number of 5.8 over a range of Reynolds numbers per inch from 97,000 to 238,000, for angles of yaw from 0° to 8°. Six combinations of the bluntness ratios 0.4, 0.8, and 1.064 with the cone half angles 10°, 20°, and 40° were used in determining the significant parameters governing pressure distribution.

The pressure distribution on the spherical nose for both yawed and unyawed bodies is predicted quite accurately by the modified Newtonian theory given by $C_p = C_{p_{max}} \cos^2 \eta$, where η is the angle between the normal to a surface element and the flow direction ahead of the bow shock. Cone half angle was found to be the significant parameter in determining the pressure distribution near the nose-cone junction and over the conical afterbody. On the 40° spherical nosed cone models the flow overexpanded with respect to the Taylor-Maccoll pressure in the region of the spherical-conical juncture, after which the pressure returned rapidly to the Taylor-Maccoll value. For models with smaller cone angles the region of minimum pressure occurred farther back on the conical portion of the model, and the Taylor-Maccoll pressure was approached more gradually. The shape of the pressure distributions as described in nondimensional coordinates was independent of the radius of the spherical nose and of the Reynolds number over the range of Reynolds number per inch between $.97 \times 10^5$ and 2.38×10^5.

Integrated results for the pressure foredrag of the models at zero yaw compared very closely with the predictions of the modified Newtonian approximation, except for models with large cone angles and small nose radii, where the drag approaches the value given by the Taylor-Maccoll theory for sharp cones.

TABLE OF CONTENTS

LIST OF SYMBOLS

C_{D_F}	foredrag coefficient, dimensionless
C_p	pressure coefficient, $\frac{p - p_\infty}{\frac{1}{2} \rho_\infty U_\infty^2}$, dimensionless
$C_{p_{max}}$	pressure coefficient at the stagnation point, dimensionless
$\bar{I}$	unit vector in the x- direction, dimensionless
$\bar{J}$	unit vector in the y- direction, dimensionless
$\bar{k}$	unit vector in the z- direction, dimensionless
M	Mach number, dimensionless
$\bar{n}$	unit vector normal to surface, dimensionless
p	air pressure, lb./sq. in.
r	nose radius, inches
R	cone base radius, inches
r/R	bluntness ratio, dimensionless
S	distance measured on the surface from the intersection of model surface with its longitudinal axis, inches
S/r	non-dimensional orifice distance
U	free stream velocity, ft./sec.
x, y, z	a right hand system of coordinate axes, fixed in the body
α	yaw angle
γ	ratio of specific heats, dimensionless
δ	shock detachment distance, inches
∇	gradient
η	angle between free stream flow direction and the normal to the body surface
θ_c	cone half angle

ρ air density, lb. sec.^{2}/ft.^{4}

σ polar angle of spherical nose

ϕ meridian angle

Subscripts

$( )_2$ static condition behind bow shock wave

$( )_\infty$ free stream conditions

$( )_o$ refers to stagnation, or reservoir conditions

$( )_j$ refers to nose-cone junction

$( )_{p.m.}$ at minimum pressure point

$( )_s$ static condition

$( )_{t_1}$ refers to total head in front of bow shock

Superscripts

$( )'$ cone half angle of tangent cone

I. INTRODUCTION

Structural problems resulting from the aerodynamic heating of slender, sharp-nosed bodies in very high speed flight may require that future hypersonic flight vehicles have blunt noses in order to provide sufficient space for heat removal apparatus. Furthermore, it has been shown by Sommer and Stark (Ref. 1), and Eggers, Resnikoff, and Dennis (Ref. 2) that for a body of revolution of a given length or volume the minimum drag at hypersonic airspeeds is obtained with a shape having a blunt nose. Hence the aerodynamics of blunt bodies in hypersonic flow is a subject of considerable current interest.

At hypersonic speeds the component of flight Mach number normal to the surface of a blunt body is much larger than unity, and the inertia forces predominate over the elastic forces in the disturbed air. But this condition is precisely that postulated by Newton in his original treatment of fluid motion, as pointed out in Reference 2. In Newton's theory the fluid is regarded as a collection of discrete particles with no interaction between particles. It admits no shock wave and hence fluid particles are unperturbed before striking the surface of a body moving through them. As each particle strikes the surface, it loses the component of its momentum normal to the body surface, while its tangential component is unchanged. The loss in normal momentum appears as an increase in pressure at the surface compared with the free stream pressure. The Newtonian pressure coefficient is

$$C_p = 2 \cos^2 \eta$$

where η is the angle between the free stream flow direction and the normal to the body surface. In the language of modern gas dynamics

Newton's analysis applies strictly in the limiting case: $M \longrightarrow \infty$ and $\gamma \longrightarrow 1$.

Newtonian theory predicts a pressure coefficient at the stagnation point, $C_{p_{max}}$, equal to 2, but in a real gas the bow shock wave produces a finite volume compression and the rest of the deceleration to the stagnation point occurs isentropically. Therefore the actual value of $C_{p_{max}}$ is somewhat less than 2, being about 1.82 for $M_\infty = 5.8$ and $\gamma = 1.4$, and 1.66 at $M_\infty = 2$. As discussed by Lees (Ref. 3), Oliver (Ref. 4), and Penland (Ref. 5), the pressure distribution over a blunt body is predicted quite accurately if the Newtonian theory is modified by introducing the normalized pressure distribution

$$C_p/C_{p_{max}} = \cos^2\eta$$

This result agrees exactly with the recent stagnation point theories of Ting-Yi Li (Ref. 6) and Hayes (Ref. 7).

Now the Newtonian approximation also predicts quite closely the value of the pressure on the surface of a semi-infinite unyawed circular cone, provided $M_\infty \sin \theta_c$ is sufficiently large. The object of the present investigation is to investigate experimentally the surface pressure distribution and shock wave shape in the intermediate region extending from the stagnation-point zone on a blunt nose to the end of a conical afterbody. Oliver (Ref. 4), in a recent study of a spherically-blunted 40° cone, observed an over-expansion below the final Taylor-Maccoll pressure value on the conical skirt, followed by a recompression to the proper asymptotic level. The present study seeks to determine

what parameters are significant in determining the length of this transition zone, as well as other main features of the flow. It also extends the comparison with the Newtonian approximation and inviscid cone theories to the case of a yawed body.

Six models in the form of truncated circular cones with tangentially connected spherical nose segments were used to obtain static pressure measurements at angles of yaw of 0°, 4°, and 8°. The parameters which were varied were cone half angle ($\theta_c = 40^{\circ}$, 20°, and 10°) and bluntness ratio, or ratio of nose radius to cone base radius($r/R = 0.4$, 0.8, and 1.064).

The tests were conducted at a nominal Mach number of 5.8 in the GALCIT 5 x 5 inch hypersonic wind tunnel.

II. EQUIPMENT AND PROCEDURE

A. Wind Tunnel

The tests were conducted in the GALCIT 5 x 5 inch hypersonic wind tunnel (leg no. 1), which is of the continuous-flow, closed-return type and can be operated with supply pressures between 1 and 6.7 atmospheres absolute. The Mach number was nominally 5.8. All tests were made at a fixed reservoir temperature of 225°F, over a range of reservoir pressures from 37 to 95 lbs. per sq. in. absolute. This temperature was selected to yield maximum Reynolds numbers per inch while insuring the absence of air condensation in the test section. A schematic diagram of the wind tunnel installation is shown in Figure 1. The test section, with one side plate removed, and two methods of model mounting are shown in Figure 2. An extensive description of the experimental facilities is given in Reference 8.

B. Description of the Models

The six brass models used in the investigation are shown in Figures 3, 4, 5, and 6. The general configuration of each model was a conical section with a spherical nose. All six models had a base radius of .875 inches. Two parameters were varied in the construction of the models; the cone semi-vertex angle and the nose radius. The following combinations of these two parameters were used:

Model	Semi-vertex angle, θ_c	Nose radius, r	Base radius, R	Bluntness ratio, r/R
1	40^o	.350"	.875"	.4
2	40^o	.700"	.875"	.8
3	20^o	.350"	.875"	.4
4	20^o	.700"	.875"	.8
5	20^o	.931"	.875"	1.064
6	10^o	.700"	.875"	.8

The fifth model represented the maximum nose radius which could be inscribed in a 20^o half angle cone having a base radius of .875 inches, and in this limiting case the geometrical shape was a simple spherical segment (Fig. 6A).

Static pressure orifices were located on the spherical and conical surfaces of each model, as shown in Figures 4, 5, and 6. These orifices, .016 inches in diameter, were drilled normal to the surface to a depth of approximately .040 inches, where they intersected larger passages drilled through the model from the rear. A typical arrangement of these internal passages is shown in Figure 7. Short lengths of stainless steel tubing were brazed into each of the holes in the rear of the model, permitting attachment of flexible saran plastic tubing which was used to connect the model to the manometers. The tubes extending from the rear of each model may be seen in Figure 3. The advantage of this type of construction was the absence of internal joints where inaccessible leaks might occur.

Two methods were used in mounting the models in the wind tunnel. For tests at zero yaw the models were mounted on an axial sting, which was supported at the rear at a point well downstream of the test section and at the front by a vertical strut from the top of the test

section (Fig. 2A). The distance between the forward support and the base of the model was $4\frac{1}{2}$ inches. To minimize disturbances to the base pressure on the model, the pressure leads were wrapped closely around the sting for some distance downstream of the model, after which they were led out of the tunnel and connected to the manometers.

For the angle of yaw tests the models were mounted on a short sting which was supported by two vertical struts from the top of the test section (Fig. 2B). The distance between the forward support and the base of the model was $3\frac{1}{2}$ inches. Differential movement of the two vertical struts by means of external controls permitted variation of the angle of yaw of the model. (Since the models were axially symmetric, the term angle of yaw as used in this discussion is synonymous with the term angle of attack.)

In both methods of mounting, the model was attached to the sting by means of a close fitting shaft and sleeve, which were machined true with the axis of the model (Fig. 7). This arrangement permitted the models to be rotated about their axes without changing the angle of yaw. A set screw maintained the models in any desired rotational position.

C. Test Procedure

All six models were tested at zero yaw, and models 1 and 4 (Figs. 4A and 5B) were tested at angles of yaw of 4° and 8°.

For the tests at zero yaw the models were positioned on the tunnel axis. The nose of each model was located 24 inches downstream of the throat. After the pressure leads were connected to the manometers the system was checked for leaks. The tunnel was operated for at

least 90 minutes before data was taken in order to allow equilibrium temperatures to be reached throughout the wind tunnel and the compressor plant. Static pressure measurements were made at a stagnation pressure of 75 psia and a stagnation temperature of 225°F., which corresponded to free stream conditions of a Mach number of 5.8 and a Reynolds number per inch of 1.91×10^5. Empty tunnel pressure surveys by previous investigators had shown a variation of total pressure up to plus or minus three per cent in the region of the tunnel used for these tests; therefore, data was taken in three rotational positions of each model spaced 90° apart around the axis of revolution.

For the tests at angles of yaw the models were initially positioned on the tunnel axis with the nose of each model located at approximately $21\frac{1}{2}$ inches downstream of the throat. Leak checks were conducted as before. The models were yawed by differential movement of the vertical supports in such a manner as to keep the nose of the model on the tunnel centerline at all times. Static pressure measurements were made at angles of yaw of 0°, 4°, and 8°, at a stagnation pressure of 95 psia and a stagnation temperature of 225°F. These stagnation conditions corresponded to free stream conditions of a Mach number of 5.8 and a Reynolds number per inch of 2.38×10^5. As shown in Figures 4A and 5B the pressure orifices were located in four meridian planes, 45° apart, through the axes of the models. When a model was mounted in the tunnel, one of the meridian planes of the model which contained the pressure orifices was aligned vertically. This meridian plane was designated as the vertical meridian plane, and this was the plane in which the model was yawed. The meridian planes containing the

other pressure orifices on the model were designated as the diagonal meridian planes and the horizontal meridian plane. For each model at a given angle of yaw it was desired to obtain pressure measurements at every orifice location in each of the four meridian planes. This aim was accomplished by taking pressure readings with the model yawed first above and then below the free stream direction in each of five rotational positions, separated by 45°. Because of the axial symmetry, this procedure was equivalent to taking measurements in ten rotational positions of each model at each angle of yaw.

In order to investigate the effect of Reynolds number variation, model 4 was also tested at zero yaw at stagnation pressures of 37 psia and 54 psia, and a stagnation temperature of 225°F. These conditions corresponded to Reynolds numbers per inch of $.97 \times 10^5$ and 1.41×10^5 respectively, and a Mach number of 5.7. These tests were identical to the previously described tests at zero yaw, except that the model was mounted on the two vertical supports, and the nose of the model was located $21\frac{1}{2}$ inches downstream of the throat.

III. RESULTS AND DISCUSSION

A. Schlieren Observations

Schlieren photographs of the flow over each of the six models at zero yaw are shown in Figures 8 through 13. For this series of observations the free stream Mach number is 5.8 and the Reynolds number per inch is 1.91×10^5, with the exception of Figure 10, for which the Mach number was 5.7 and the Reynolds number per inch was $.97 \times 10^5$. In general it may be seen that the shock waves lie close to the bodies as is characteristic of hypersonic flow. The shape of the shock waves for the more blunt models, such as model 4 (Fig. 11), is dominated by the effect of the blunt nose, whereas for the more pointed models, such as model 1 (Fig. 8), the shock shape is dominated by the conical portion of the model. A peculiarity which is particularly apparent in Figure 8 and shows slightly in Figure 9 is the reverse curvature in the shock wave midway out on the conical portions of models 1 and 2. This condition was observed only on these two 40° half angle models, and it was closely connected with the over-expansion and recompression on the conical portions of these models (see discussion of static pressure measurements at zero yaw).

The separation distance, δ, of the bow shock wave from the nose of each model at zero yaw, as measured from the schlieren photographs, is compared with the radius of the spherical nose of the model in the following table:

Model	δ, inches	r, inches	δ/r
1	.0594	.350	.169
2	.1153	.700	.165
3	.0592	.350	.169
4	.1121	.700	.160
5	.1496	.931	.161
6	.1098	.700	.157
		Average =	.164

From this table it is apparent that the variation of shock separation distance with the radius of the nose of the model was essentially linear. Theoretical analyses have been made by Heybey (Ref. 9), Hayes (Ref. 7), and Li and Geiger (Ref. 6) to predict the bow shock wave separation distance for blunt bodies in hypersonic flow. Heybey's analysis gives the shock separation distance in front of a sphere at a Mach number of 5.8 as $\delta/r = .138$, including the correction for compressible flow behind the bow shock. Hayes' analysis, which assumes the density ratio across the bow shock wave, ρ_∞/ρ_2, to be very small and also assumes incompressible flow behind the shock, gives a value of $\delta/r = .118$. The analysis by Li and Geiger, which also assumes a very small density ratio and incompressible flow behind the shock, predicts a value of $\delta/r = .137$ for the conditions of the present experiment. Since the density ratio across a bow shock wave at a Mach number of 5.8 is .192, which is not very small with respect to 1.0, the agreement between the present results and the foregoing theoretical predictions is considered fair.

The schlieren photographs of models 1 and 4 at angles of yaw of 4° and 8° are shown in Figures 14 through 17. For these observa-

tions the free stream Mach number was 5.8 and the Reynolds number per inch was 2.38×10^5. The shock wave shapes for the yawed models were generally quite similar to those for the same models at zero yaw, except for the slight asymmetry introduced by the angle of yaw.

B. Surface Pressure Distribution

1. Unyawed Bodies

The pressure distributions at a Mach number of 5.8 and a Reynolds number per inch of 1.91×10^5 for each of the six models at zero yaw are plotted in Figures 18 through 23 in the form $C_p/C_{p_{max}}$ versus S/r, where S is the arc length along the surface of the model measured from the axis of symmetry, and r is the radius of the spherical nose of the model. Along the spherical surface, S/r corresponds to the polar angle in radians, and along the conical surface, S/r corresponds to a dimensionless linear distance. In obtaining these results for $C_p/C_{p_{max}}$ the three sets of pressure data for each model were reduced separately and then averaged to give a mean value for the pressure coefficient at each orifice location on the model. Also plotted in Figures 18 through 23 are the values for $C_p/C_{p_{max}} = \cos^2 \eta$ based on the modified Newtonian approximation. For the conical portions of the models the Taylor-Maccoll values of $C_p/C_{p_{max}}$ computed from the Kopal tables (Ref. 10) for inviscid supersonic flow over cones are shown for comparison. In order to bring out the effect of bluntness ratio, r/R, with cone half angle held constant, the data of Figures 18 and 19 for $\theta_c = 40^\circ$ are replotted in Figure 24. Likewise the data of Figures 20 through 22 for $\theta_c = 20^\circ$ are replotted in Figure 25.

a. Spherical Nose

Close agreement between experimental pressures and Newtonian theory is evident on the spherical nose of each model. In each case, however, the test data fall slightly below the theory in the region of most rapidly changing pressure. The deviation is usually only a few per cent, in some instances approaching a maximum of only 10 per cent. In the region approaching the junction between the spherical nose and conical afterbody some models show a marked deviation associated with local effects.

b. Nose-Cone Junction and Conical Skirt

Examination of Figures 24 and 25 shows that bluntness ratio itself has very little effect on the surface pressure distribution and that the half-angle of the conical skirt is the dominant geometric parameter. A pressure minimum downstream of the nose-cone junction is found on the 40° conical skirt, as in Oliver's tests, but this minimum moves a considerable distance aft when the cone half angle is reduced to 20°. This behavior agrees with qualitative predictions based on previous theoretical studies of blunt bodies at hypersonic speeds. For large cone half-angles the pressure on the spherical nose just upstream of the nose-cone junction should be given very closely by the modified Newtonian approximation, because $M_{\infty} \sin \theta_c >> 1$. For example, at $M_{\infty} = 5.8$ and $\gamma = 1.4$, $C_{p_j} \cong 1.82 \sin^2 \theta_c$. But the Taylor-Maccoll value of the pressure on the conical skirt far downstream is approximately $2.08 \sin^2 \theta_c$ for $M_{\infty} \longrightarrow \infty$,* so that C_{p_j} should lie below

* At $M_{\infty} = 5.8$ the actual value is even higher.

this asymptotic value. Therefore one would expect to find a pressure minimum on the skirt for large cone half-angles, followed by a recompression to the Taylor-Maccoll conical shock angle far downstream. (Figure 8) Since the drag/length of the skirt is high the pressure minimum occurs relatively close to the nose-cone junction.

For smaller conical half angles the nose drag begins to dominate the flow pattern, and the surface pressure is expected to approach the monotonically-decreasing pressure distribution typical of the limiting case of a hemisphere-cylinder ($\theta_c = 0$) for $M_\infty > 3.50$ (air) as explained by Lees (Ref. 11). That such behavior does exist for hemisphere-cylinders has been shown experimentally by Oliver (Ref. 4), for example. At $M_\infty = 5.8$ the pressures were shown to depart from Newtonian values on the spherical nose near the junction with the cylindrical afterbody. Similarly the pressures on the blunted cones of small half-angle should be somewhat higher than Newtonian near the nose-cone junction. Figure 23 shows this behavior for $\theta_c = 10^\circ$. At the same time the skirt drag is not comparable with the nose drag until the skirt length is several nose diameters long. For both of these reasons the pressure minimum moves rapidly aft with decreasing θ_c. A critical value of the half-angle exists below which the pressure minimum no longer occurs. In these tests this angle was approximately 20°. It should be pointed out that this critical angle decreases with decreasing Mach number below 5.8, and for $M_\infty < 3.5$ (air), overexpansion occurs even on the hemisphere-cylinder.

Neglecting viscous effects, one would not expect the nose-skirt junction to influence the pressure upstream unless the Mach wave from the junction strikes the sonic line. At the junction the normal pressure

gradient is discontinuous, and the corresponding discontinuity in pressure gradient along the surface is given by

$$\Delta\left(\frac{d\,C_p/C_{p_{max}}}{dS/r}\right) = + \frac{\gamma M^2}{\sqrt{M^2 - 1}} \left(\frac{C_p}{C_{p_{max}}} + \frac{2}{\gamma M_\infty^2} \quad \frac{1}{C_{p_{max}}}\right)$$

For all the conditions of the present series of experiments this discontinuity in

$$\frac{d\,C_p/C_{p_{max}}}{d\,S/r}$$

would reduce the negative surface pressure gradient, but would not reverse its sign. Now, examination of Figures 23 through 25 shows that the nose-cone junction influences the surface pressure upstream to an extent that cannot be explained by deviations from the Newtonian distribution. For example, the pressure coefficient at the junction is only 5 per cent above Newtonian for 40° cones, but is 37 per cent higher for 20° cones, and 146 per cent higher for 10° cones. The deviation can be explained, at least in part, by model surface irregularities which naturally occur at the nose-cone junction because of the difficulty in fabricating the desired "jump" in radius of curvature. Any gradual fairing in of the spherical nose with the conical skirt will reduce the negative surface pressure gradient on the nose and consequently raise the entire level of the downstream pressure distribution.

The data of Figures 18 and 21 and also Figures 24 and 25 do not show any significant Reynolds number effects over the range tested.

2. Yawed Bodies

Surface pressure distributions for models 1 and 4 at a yaw angle of 8° are shown in Figures 26 through 31. In obtaining the results for the tests at angles of yaw, the data recorded for the three different rotational positions of each model were reduced separately and then combined to give a value for the pressure coefficient at each orifice location. Both $C_p/C_{p_{max}}$ and the quantity $\cos^2\eta$ are again plotted versus the non-dimensional orifice distance, S/r. The angle, η, in the yaw tests is no longer a simple function of body geometry, but is a function of angle of yaw as well, and this angle was computed by the procedure given in the Appendix. To give adequate representation of the three-dimensional aspects introduced by yawed bodies, pressure distribution is plotted along four meridian planes. These planes are orientated as follows: (1) one plane is vertical; (2) two planes, referred to as diagonal meridian planes, lie in positions defined by the meridian angle ϕ, and are 45° and 315° from the vertical meridian plane; (3) one plane is horizontal. Because of symmetry, the data obtained on the two diagonal planes have been averaged and plotted as for one plane. Likewise, the data obtained on the two halves of the horizontal plane have also been averaged and plotted for one half of the plane. Values of $C_p/C_{p_{max}}$ for a yawed cone, as given by the Stone-Kopal first order theory (Ref. 12), are also plotted over the conical portion of each model.

a. Spherical Nose

Yaw data show the same close agreement with the modified Newtonian approximation on the spherical nose as in the zero yaw case.

In the region of most rapidly changing pressures, the experimental results again show slightly lower pressures than the theory. It is of importance to note at this point that in the yawed tests, except for the vertical meridian plane, the pressures obtained at orifices along a particular geometric ray are not pressure along one streamline, but are pressures obtained on many different streamlines. Hence, the modified Newtonian law holds over the entire surface in any direction for a spherical nose.

b. Nose-Cone Junction and Conical Skirt

In order to bring out the effects of yaw, the data of Figures 26 through 29 are replotted in Figure 32. Examination shows the downstream movement of the minimum pressure point as half angle is decreased. Here it is convenient to utilize a concept somewhat analogous to the tangent cone approximation. The upper and lower conical rays in the vertical meridian plane may be regarded at the various angles of yaw tested as belonging to two other cones at zero yaw whose half angles are given by the relations,

$$\theta_c' = \theta_c + \alpha \qquad \text{(lower half plane)}$$

$$\theta_c' = \theta_c - \alpha \qquad \text{(upper half plane)}$$

For the two models, at $\alpha = 8^\circ$, four cones may be considered whose half angles are 12°, 28°, 32°, and 48°. Presumably, the 28° cone, represented in the lower half meridian plane of model 4, would have a minimum pressure point were its skirt to be sufficiently increased in length, since its pressures lie below the Stone-Kopal values on the cone. On the other hand the pressure distribution over the 12° tangent cone, lies above the Stone-Kopal value, and is very similar to that

shown for the 10° cone (Figure 23). The yaw data confirm the zero yaw result in that the critical value of θ_c, below which there is no minimum pressure point, lies between a half angle of 28° and 12°.

Further evidence of the downstream movement of the pressure minimum as θ_c is decreased is revealed by Figure 33, which shows data for the vertical meridian plane of model 1 at angles of yaw of 0°, 4°, and 8°. The tangent cones have values of $\theta_c = 32^{\circ}$, 36°, 40°, 44°, and 48°. The location of the pressure minimum point downstream of the nose-cone junction in numbers of nose radii for various cone half angles is summarized in the table following:

θ_c or θ_c'	$(S/r)_{p.m.} - (S/r)_j$
48°	0.06
44°	0.09
40°	0.15
36°	0.25
32°	0.40
20°	2.28

When the cone skirt is sufficiently long the data show that the pressures approach the tangent cone values more closely than the values given by the Stone-Kopal first-order theory. Also shown in Figure 33 is the fact that $(C_p/C_{p_{max}}) - (C_p/C_{p_{max}})_{\alpha=0}$ varies linearly over the range of yaw angles tested.

Variation of $C_p/C_{p_{max}}$ with meridian angle is shown in Figure 34 as replotted from Figures 26 through 28.

C. Drag at Zero Yaw

The pressure distributions for each of the six models at zero yaw were integrated to obtain the pressure drag on the spherical and conical portions of the models. The results are plotted in Figure 35 as the foredrag coefficient referred to the base area, C_{D_F}, versus the bluntness ratio, r/R, with the cone semivertex angle as a parameter. Also shown for comparison are the foredrag coefficients for 10°, 20°, and 40° spherical nosed cones computed from the modified Newtonian approximation. For the relation $C_p = C_{p_{max}} \cos^2 \eta$, the foredrag coefficient of any spherical nosed cone is given by the formula

$$C_{D_F} = C_{p_{max}} \left[\tfrac{1}{2} \cos^4 \theta_c \, (r/R)^2 + \sin^2 \theta_c \right] .$$

In addition the foredrag coefficients are shown for 10°, 20°, and 40° semivertex angle cones as computed from the Kopal tables (Ref. 10), as well as the foredrag coefficient of a hemisphere-cylinder as computed from the data of Reference 4. Except for models with large cone angles and small bluntness ratios, the pressure drag of all the spherical nosed cones was given very closely by the modified Newtonian approximation. For large cone angles combined with large bluntness ratios, such as $\theta_c = 40^\circ$, $r/R = 0.8$, the pressure drag of the spherical nosed cone was greater than the drag of the hemisphere-cylinder.

IV. CONCLUSIONS

On the basis of the foregoing results it was concluded that for the range of conditions of the present investigation the pressure distributions over spherically blunted cones at zero yaw and at small angles of yaw agreed very closely with the modified Newtonian approximation, $C_p = C_{p_{max}} \cos^2 \eta$, on the spherical portions. On the conical portions the pressure distributions agreed reasonably well with the theoretical results for inviscid supersonic flow over cones as tabulated by Kopal. The only factor which influenced the deviations from the Newtonian and the Kopal predictions was the semivertex angle of the conical portion. For large cone half angles, of the order of 40°, there was a marked overexpansion with respect to the inviscid cone theory value in the region of the juncture of the conical and the spherical portions of the model, but the pressure returned fairly rapidly to the inviscid theory value on the conical portion. As the cone angle was decreased the pressure at the spherical-conical juncture increased with respect to the Kopal prediction; the region of minimum pressure occurred farther back on the conical portion; and the pressure on the conical portion approached the Kopal value much more gradually. The effects of angles of yaw on the pressure distributions were linear up to yaw angles of 8°, and in the vertical meridian plane the effect of an angle of yaw was similar to the effect of a change in the semivertex angle of the conical portion of the model. Variation of the ratio of the nose radius to the base radius produced no effect on the shape of the pressure distribution when described in nondimensional coordinates.

There was no noticeable effect of Reynolds number on the pressure distribution over the range of conditions tested.

Schlieren observations showed that for the more blunt models the shock wave shape was dominated by the effects of the blunt nose, whereas for the more pointed models the shock shape was dominated by the conical portion of the model. The separation distance of the shock wave from the nose of the models at zero yaw varied linearly with the radius of the spherical nose of the model.

Drag coefficients obtained by integrating the unyawed pressure distributions for each of the models compared very closely with the predictions of the modified Newtonian approximation, except for models with large cone angles and small nose radii, where the drag coefficients approached the values given by the Taylor-Maccoll theory for sharp-nosed cones.

REFERENCES

1. Sommer, S. C., and Stark, J. A.: The Effect of Bluntness on the Drag of Spherical-Tipped Truncated Cones of Fineness Ratio 3 at Mach Numbers 1.2 to 7.4. NACA RM A52B13, April, 1952.

2. Eggers, A. J., Resnikoff, M. M., and Dennis, D. H.: Bodies of Revolution Having Minimum Drag at High Supersonic Airspeeds. NACA TN 3666, February, 1956.

3. Lees, Lester: Hypersonic Flow. Institute of the Aeronautical Sciences, Preprint No. 554, June, 1955.

4. Oliver, Robert E.: An Experimental Investigation of Flow over Simple Blunt Bodies at a Nominal Mach Number of 5.8. GALCIT Hypersonic Wind Tunnel Memorandum No. 26, June 1, 1955. Also, J. of the Aero. Sci., Vol. 23, No. 2, February, 1956.

5. Penland, Jim A.: Aerodynamic Characteristics of a Circular Cylinder at Mach Number 6.86 and Angles of Attack up to 90°. National Advisory Committee for Aeronautics, R. M. L54A14, March 11, 1954.

6. Li, Ting-Yi, and Geiger, R. E.: Stagnation Point of a Blunt Body in Hypersonic Flow. Institute of the Aeronautical Sciences, Preprint No. 629, January, 1956.

7. Hayes, W. D.: Some Aspects of Hypersonic Flow. Ramo-Wooldridge Corporation, January, 1955.

8. Eimer, M.: Direct Measurement of Laminar Skin Friction at Hypersonic Speeds. GALCIT Hypersonic Wind Tunnel Memorandum No. 16, July 1, 1953.

9. Heybey, W. H.: Shock Distances in Front of Symmmetrical Bodies. NAVORD Report 3594, December, 1953.

10. Staff of the Computing Section, Center of Analysis, Massachusetts Institute of Technology, under the direction of Zdenek Kopal: Tables of Supersonic Flow Around Cones. Technical Report No. 1, 1947.

11. Lees, Lester: Inviscid Hypersonic Flow over Blunt-Nosed Slender Bodies. GALCIT Hypersonic Wind Tunnel Memorandum No. 31, February 1, 1956.

12. Staff of the Computing Section, Center of Analysis, Massachusetts Institute of Technology, under the direction of Zdenek Kopal: Tables of Supersonic Flow around Yawing Cones. Technical Report No. 3, 1947.

APPENDIX

A. Computation of $\cos^2 \eta$ at Angles of Yaw

The angle, η , is a function of the angle of yaw as well as of a function of surface geometry. The spherical nose and the cone skirt are treated separately.

The equation of a sphere in rectangular coordinates with the origin of the axes at the center of the sphere is given by:

$$f = x^2 + y^2 + z^2 - r^2 = 0$$

The unit vector normal to the sphere is given by the quotient of the gradient of the surface and the absolute value of the gradient. Hence,

$$\bar{n} = \frac{\nabla f}{|\nabla f|}$$

where $\nabla f = \bar{i}\, 2x + \bar{j}\, 2y + \bar{k}\, 2z$

and

$$|\nabla f| = 2(x^2 + y^2 + z^2)^{\frac{1}{2}}$$

Therefore,

$$\bar{n} = \frac{\bar{i}x + \bar{j}y + \bar{k}z}{r}$$

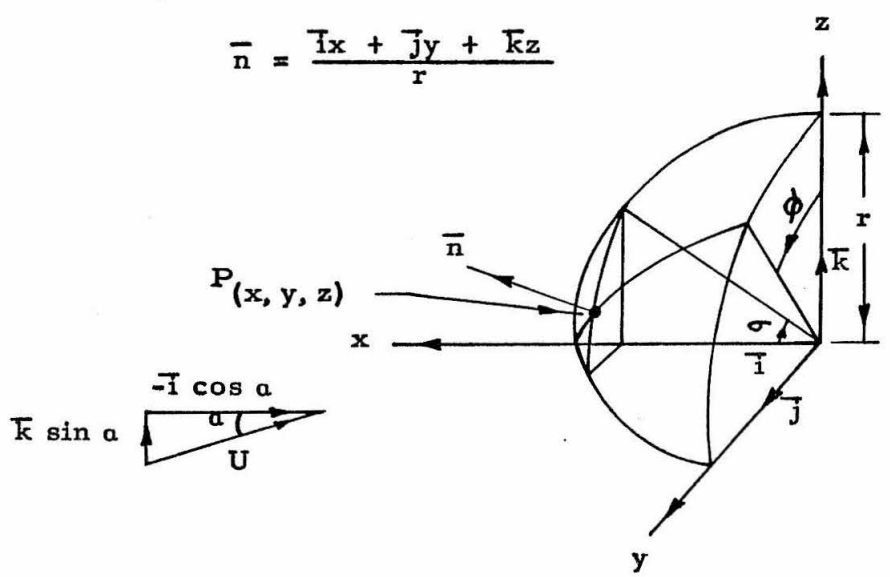

From the sketch the following quantities are defined:

$\alpha \equiv$ angle of yaw in the z- plane

$\sigma \equiv$ polar angle measured from the x- axis

$\phi \equiv$ meridian angle measured counterclockwise on the base of spherical nose segment from the vertical z- axis

Any point on the surface is defined by the coordinates x, y, z, where

$$x = r \cos \sigma$$

$$y = r \sin \sigma \sin \phi$$

$$z = r \sin \sigma \cos \phi$$

The angle of yaw in the z- plane is given by

$$\bar{a} = -\bar{i} \cos \alpha + \bar{k} \sin \alpha$$

Then $\cos \eta$ is defined as

$$\cos \eta = -\bar{n} \cdot \bar{a}$$

where $-\bar{n}$ is the inner unit normal at any point, P.

Hence,

$$\cos \eta = -\bar{n} \cdot \bar{a} = -\sin \alpha \sin \sigma \cos \phi + \cos \alpha \cos \sigma$$

The equation of the cone is

$$f_1 = x^2 \tan \theta_c - y^2 - z^2 = 0$$

where θ_c is the cone half angle.

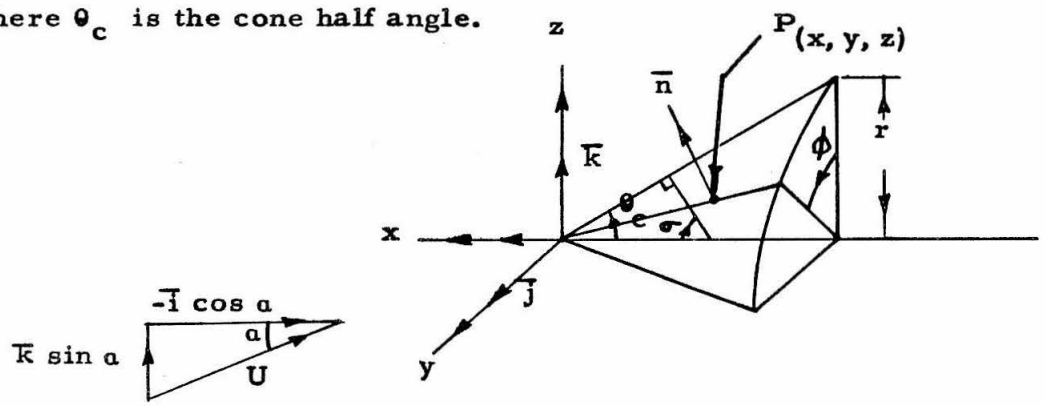

From the sketch, any point, P, on the surface is defined by the coordinates x, y, z, where

$$r = -x \tan \theta_c$$

$$y = r \sin \phi$$

$$z = r \cos \phi$$

$$y/x = -\sin \phi \tan \theta_c$$

$$z/x = -\cos \phi \tan \theta_c$$

From which

$$\bar{n} = \frac{\nabla f_1}{|\nabla f_1|} = \frac{2(\bar{I}\, x \tan^2 \theta_c - \bar{J}y - \bar{K}z)}{2(x^2 \tan^4 \theta_c + y^2 + z^2)^{\frac{1}{2}}}$$

$$\bar{n} = \frac{\bar{I}x \tan^2 \theta_c - \bar{J}y - \bar{K}z}{x \tan \theta_c \sec \theta_c}$$

$$\bar{n} = \bar{I} \sin \theta_c + \bar{J} \cos \theta_c \sin \phi + \bar{K} \cos \theta_c \cos \phi$$

Hence,

$$\cos \eta = -\bar{n} \cdot a = -\cos \theta_c \cos \phi \sin a + \sin \theta_c \cos a$$

where

$$\sigma = \frac{\pi}{2} - \theta_c$$

at the junction of the spherical segment and the cone.

B. Accuracy Considerations

1. Measured Quantities

The following is a list of possible sources of error in the measured static pressure, p_s, and reservoir pressure, p_{t_1}:

(1) Reading errors

(2) Orifice diameter

(3) Orifice location errors

(4) Angle of yaw errors

(5) Meridian angle errors

The maximum random manometer reading error was estimated to be $\pm$ 0.3 per cent of the stagnation pressure for a reservoir pressure of 80 lbs. per sq. in. gage. Orifice diameter was designed to give a maximum pressure variation from the mean of $\pm$ 2.5 per cent of the stagnation pressure. However, it is assumed that pressure transmitted to the manometer varied by a negligible amount from the mean pressure across the orifice. Deviations from designed orifice positions were such as to produce errors no larger than $\pm$ 0.5 per cent of stagnation pressure. Errors caused by angle of yaw and meridian angle setting errors were negligible.

a. Static Pressure, p_s

Total error in p_s is given as follows:

Reading error	$\pm$ 0.3 per cent
Orifice size	$\pm$ 0.0 per cent
Variation in orifice position	$\pm$ 0.5 per cent
Total error in p_s	$\pm$ 0.8 per cent

b. Reservoir Pressure, p_{t_1}

The maximum error in reading the correct value of reservoir pressure was $\pm$ 0.5 per cent of stagnation pressure.

2. Computed Quantities

As the result of errors in measurements, the computed quantities had errors as follows:

$p_\infty = \pm$ 0.03 per cent of stagnation pressure

$M_\infty = \pm$ 0.01

3. Plotted Quantities

As the result of the errors noted above, the plotted values of $C_p/C_{p_{max}}$ contained maximum errors as follows:

Region of Model	Model No.	Fraction of $C_p/C_{p_{max}}$
Nose to S/R $\cong$ 0.2	all	$< \pm$ 0.01
S/r $\cong$ 0.2 to nose-cone junction	1, 3	$\pm$ 0.012
s/r $\cong$ 0.2 to nose-cone junction	2, 4, 5, 6	$\pm$ 0.01
Cone skirt	all	$< \pm$ 0.01

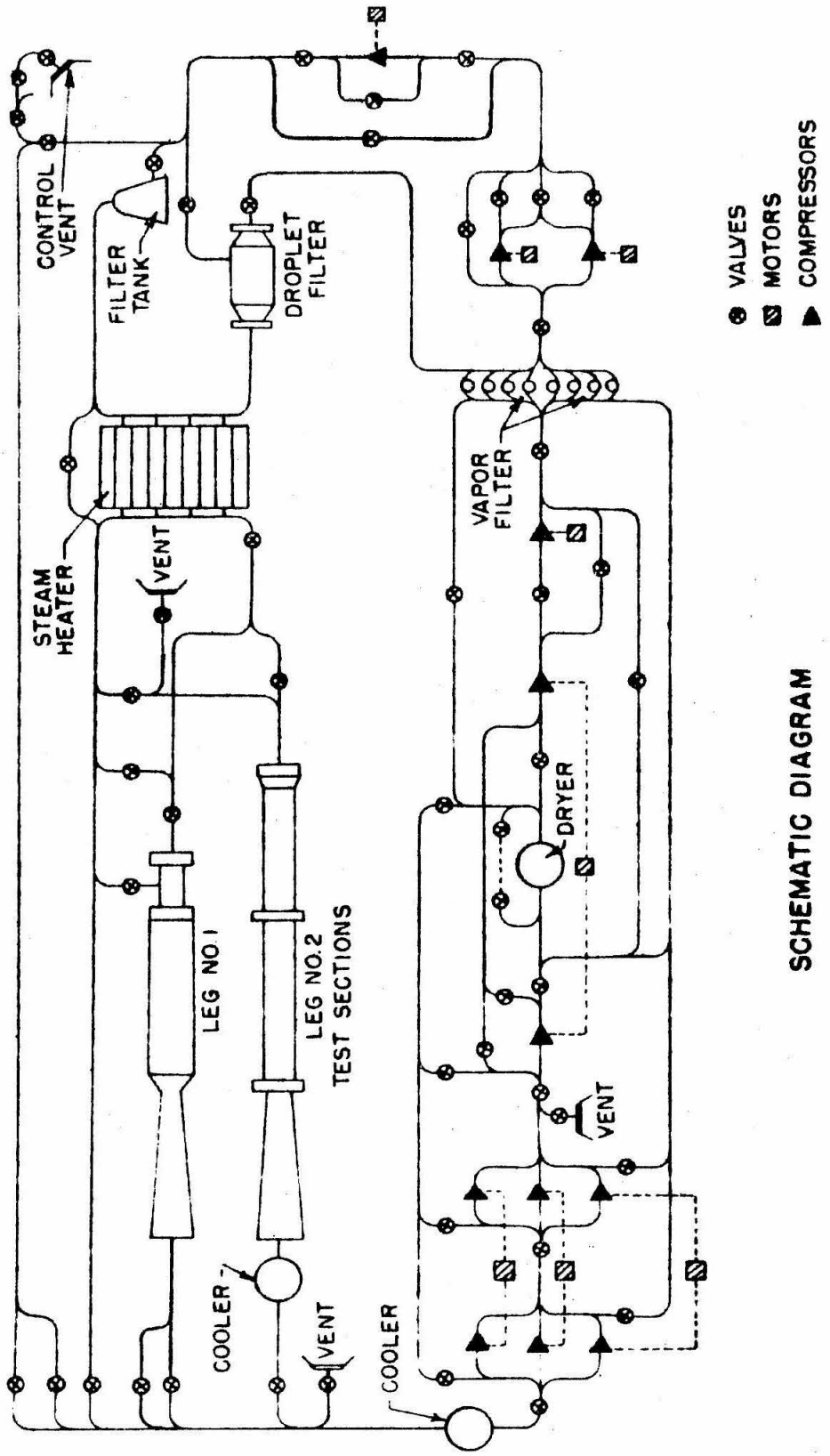

SCHEMATIC DIAGRAM

OF GALCIT 5x5in. HYPERSONIC WIND TUNNEL INSTALLATION

FIG. 1

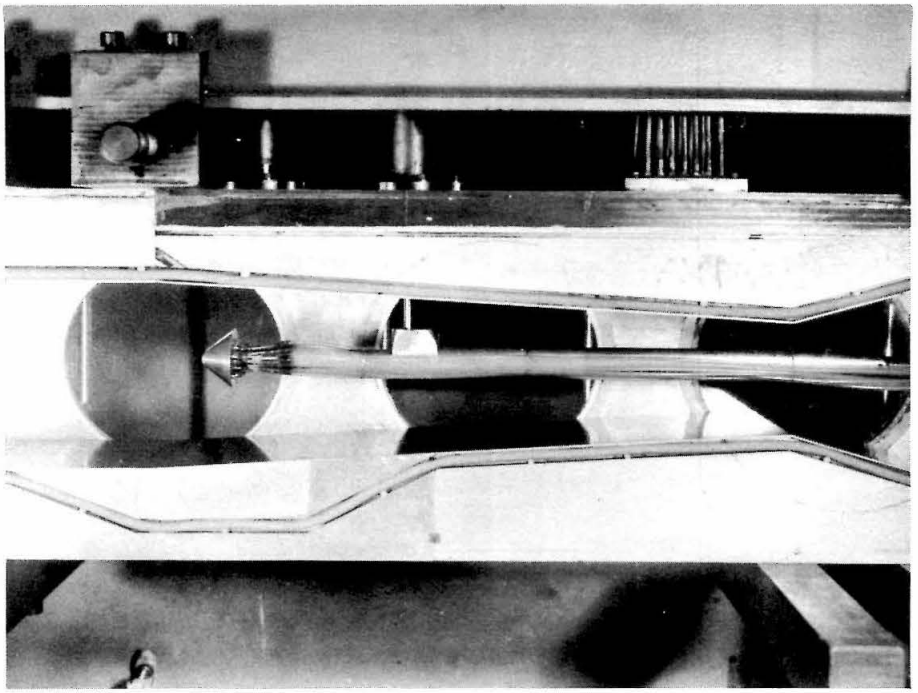

(A)

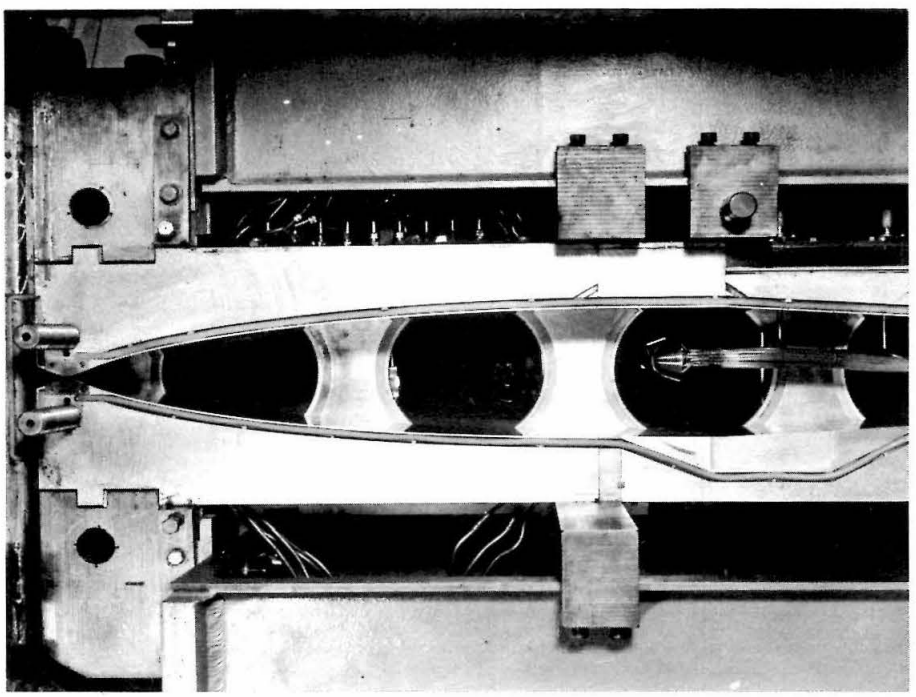

(B)

FIG. 2

TEST SECTION OF HYPERSONIC TUNNEL

SHOWING METHODS OF MOUNTING MODELS

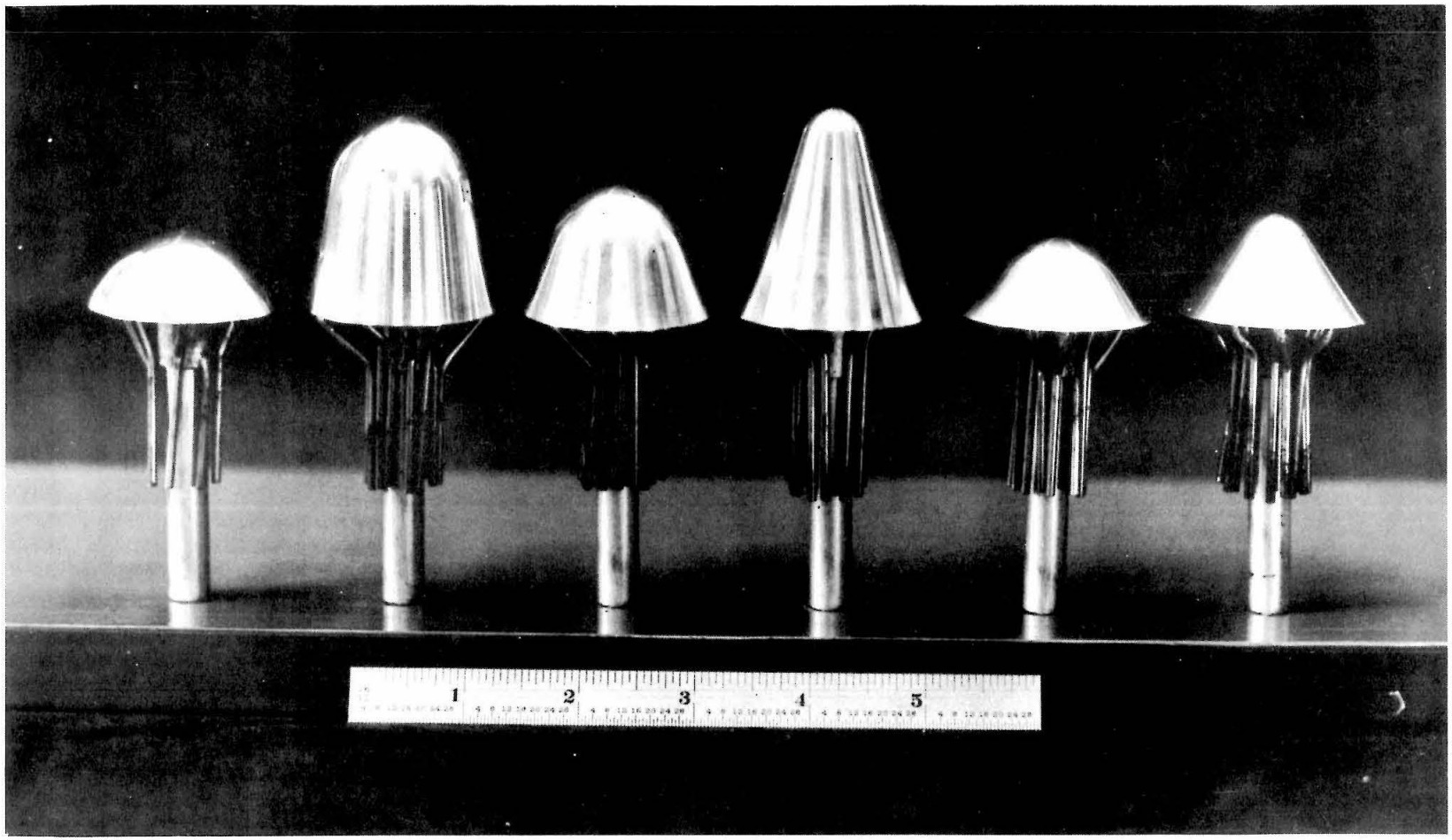

FIG. 3

SPHERICAL NOSED CONE STATIC PRESSURE MODELS

Orifice	S(in.)
1	0
2	0.070
3	0.105
4	0.140
5	0.210
6	0.210
7	0.280
8	0.315
9	0.350
10	0.385
11	0.420
12	0.490
13	0.630
14	0.805
15	0.980
16	1.155

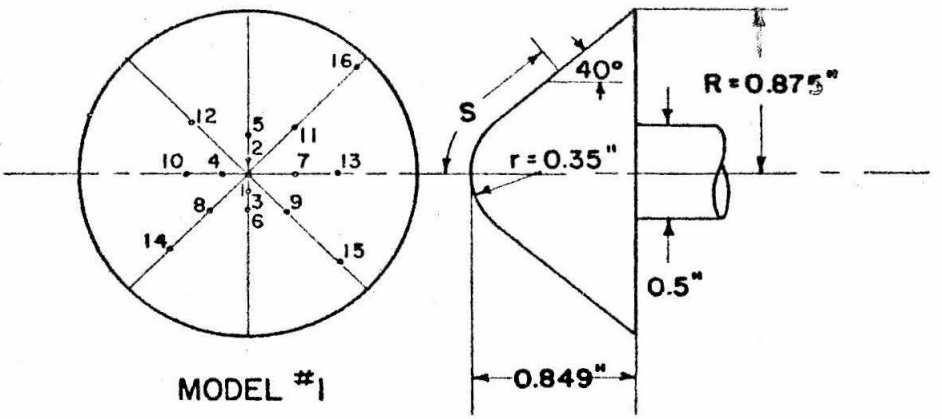

(A) 40° HALF ANGLE CONE

r/R = 0.4

Orifice	S(in.)
1	0
2	0.070
3	0.140
4	0.210
5	0.280
6	0.420
7	0.420
8	0.560
9	0.630
10	0.700
11	0.770
12	0.840
13	0.980

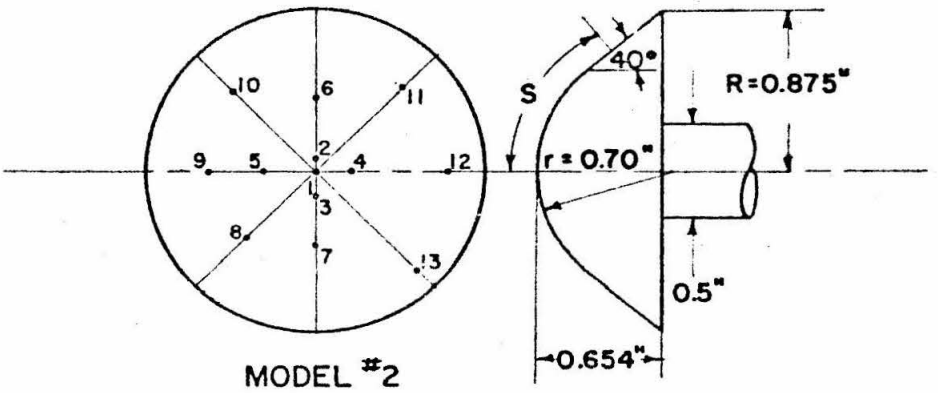

(B) 40° HALF ANGLE CONE

r/R = 0.8

FIG. 4

Orifice	S(in.)
1	0
2	0.105
3	0.175
4	0.280
5	0.385
6	0.490
7	0.595
8	0.735
9	0.735
10	0.875
11	1.155
12	1.435
13	1.715

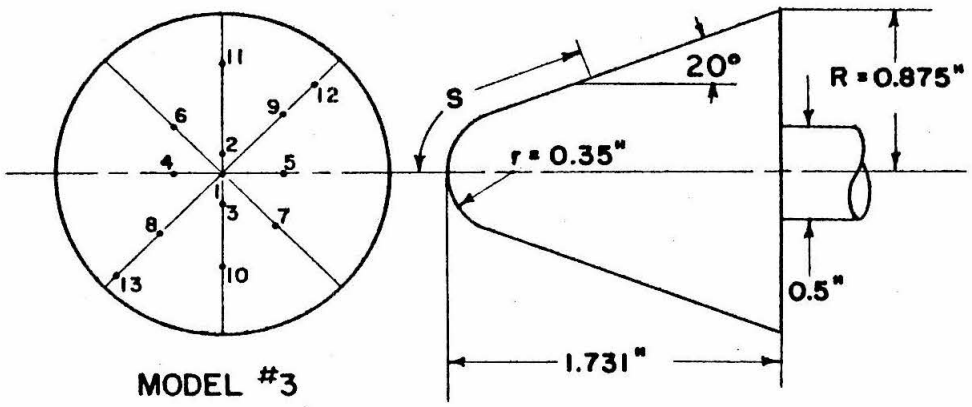

(A) 20° HALF ANGLE CONE

r/R = 0.4

Orifice	S(in.)
1	0
2	0.070
3	0.140
4	0.210
5	0.280
6	0.490
7	0.490
8	0.700
9	0.840
10	0.910
11	0.980
12	1.050
13	1.120
14	1.260

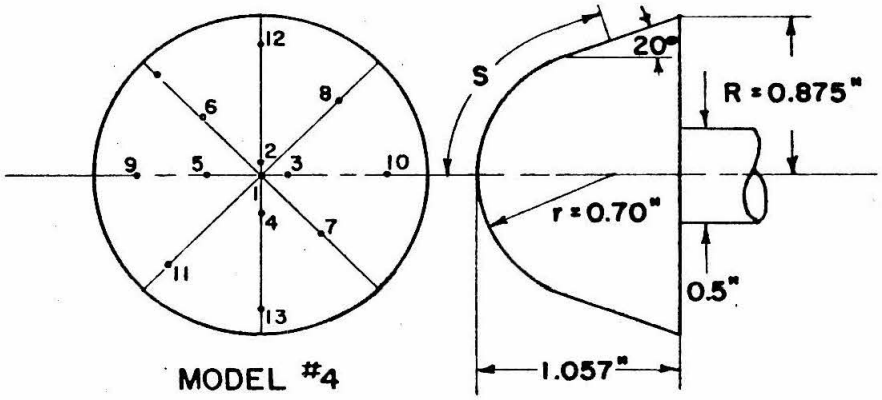

(B) 20° HALF ANGLE CONE

r/R = 0.8

FIG. 5

Orifice	S(in.)
1	0
2	0.093
3	0.186
4	0.279
5	0.372
6	0.650
7	0.650
8	0.931

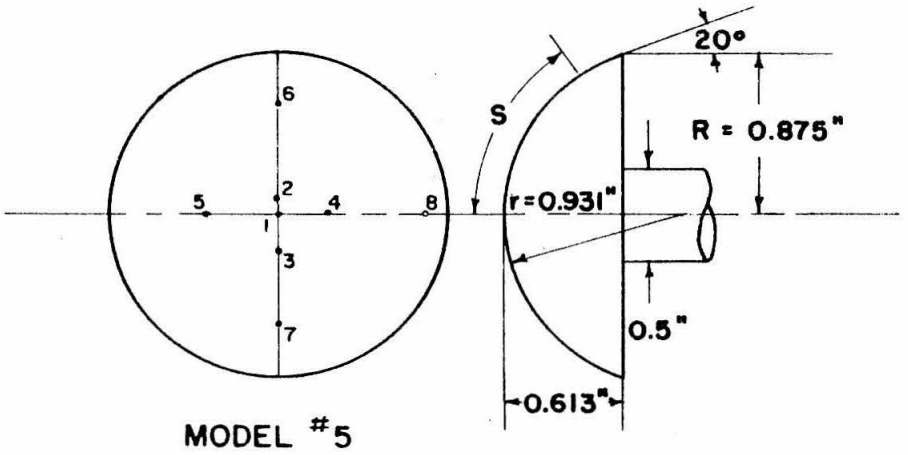

MODEL #5

(A) 20° SPHERICAL SEGMENT

r/R = 1.064

Orifice	S(in.)
1	0
2	0.070
3	0.140
4	0.210
5	0.338
6	0.420
7	0.420
8	0.630
9	0.840
10	0.910
11	0.980
12	1.050
13	1.120
14	1.260
15	1.540
16	1.820

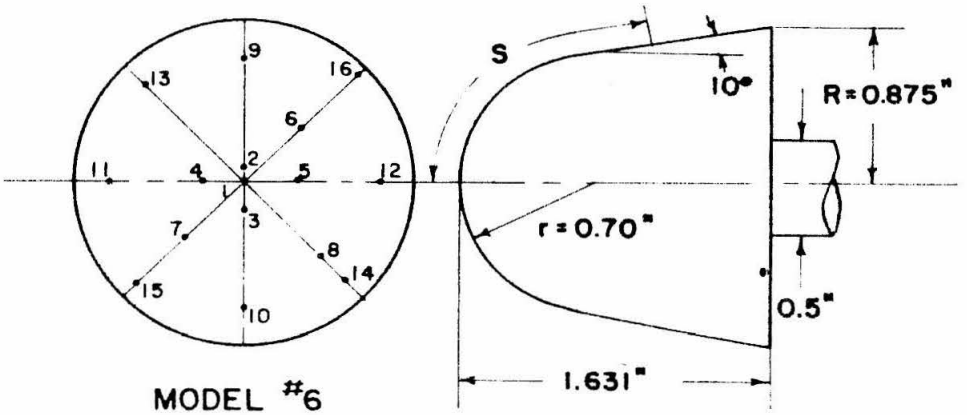

MODEL #6

(B) 10° HALF ANGLE CONE

r/R = 0.8

FIG. 6

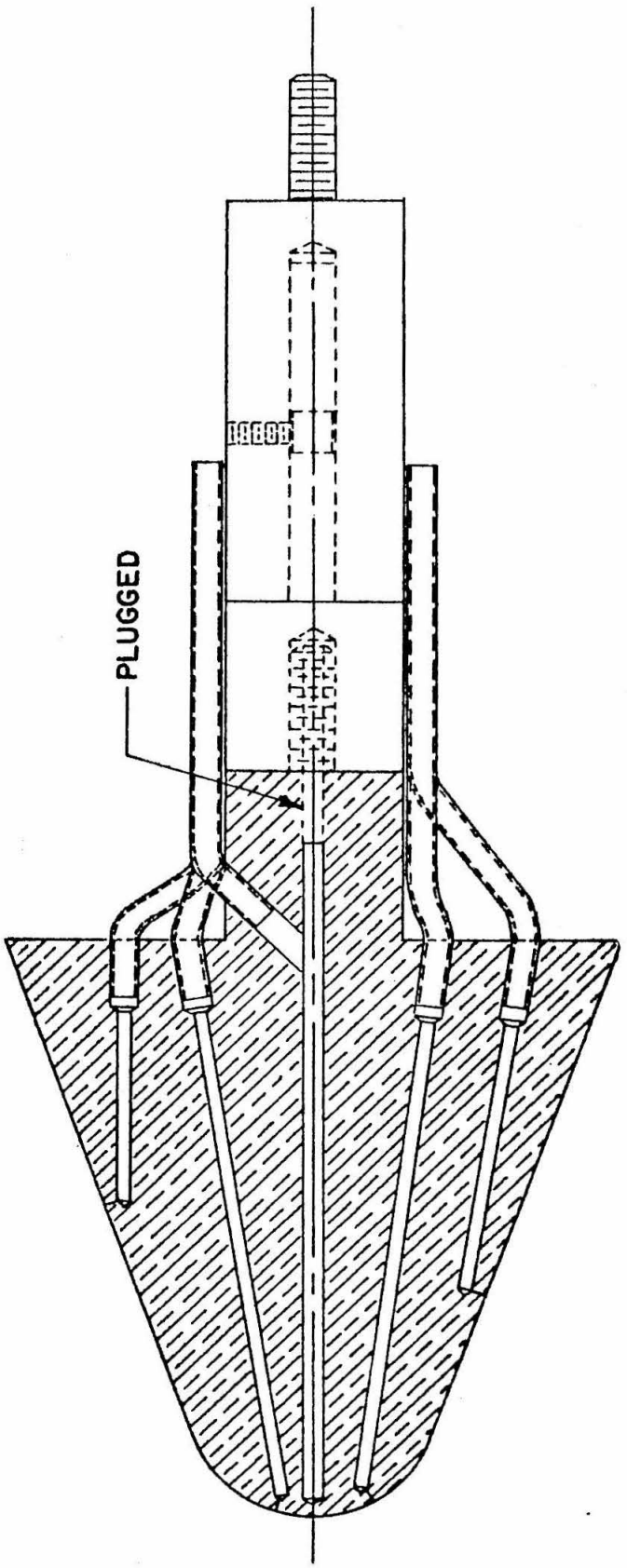

FIG. 7 DETAILS OF TYPICAL MODEL CONSTRUCTION

FIG. 8

SCHLIEREN PHOTOGRAPH OF 40° HALF ANGLE CONE

$r/R = 0.4$, $\alpha = 0^{\circ}$

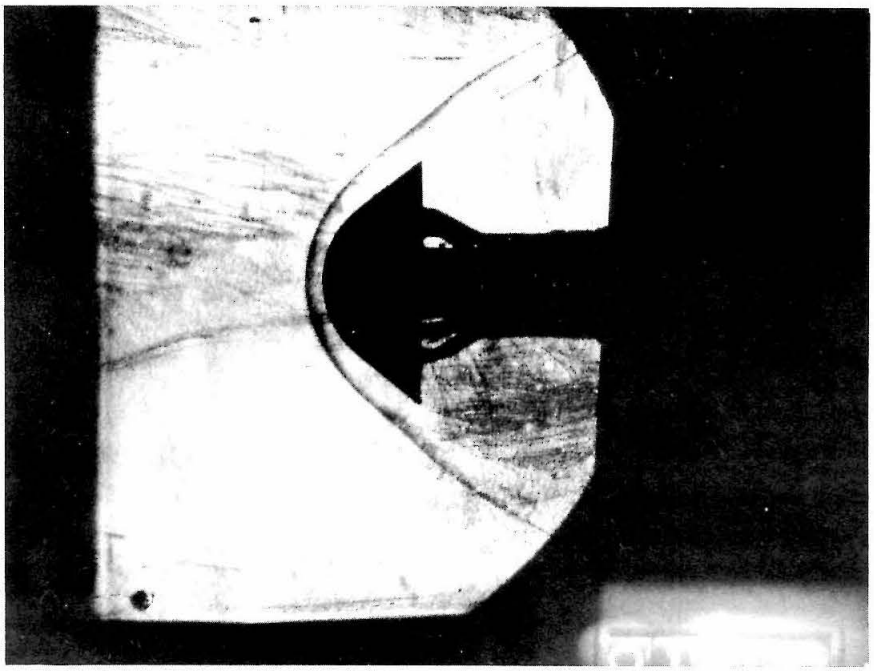

FIG. 9

SCHLIEREN PHOTOGRAPH OF 40° HALF ANGLE CONE

$r/R = 0.8$, $\alpha = 0^{\circ}$

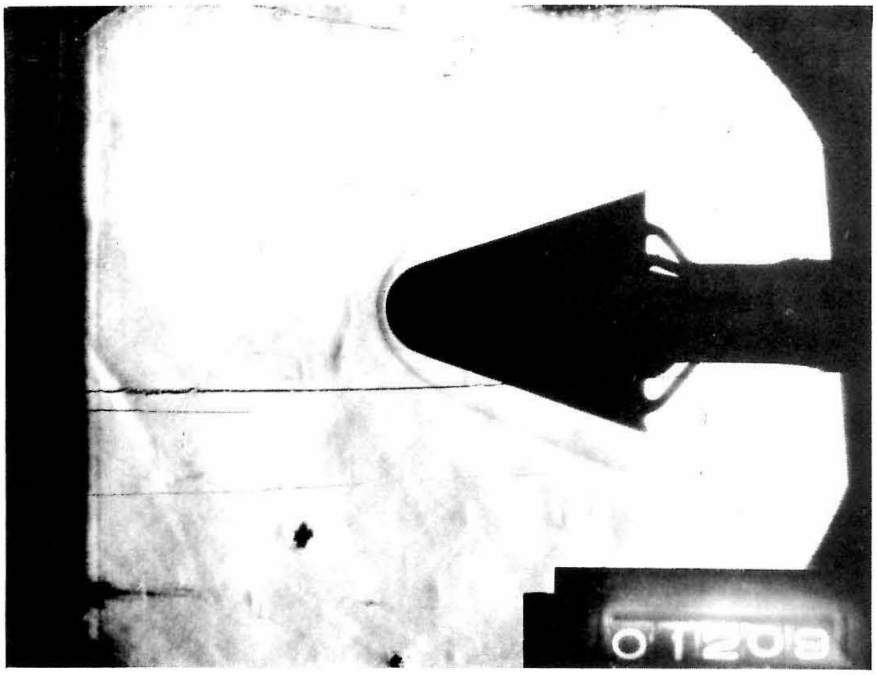

FIG. 10

SCHLIEREN PHOTOGRAPH OF 20° HALF ANGLE CONE

r/R = 0.4, $\alpha = 0^{\circ}$

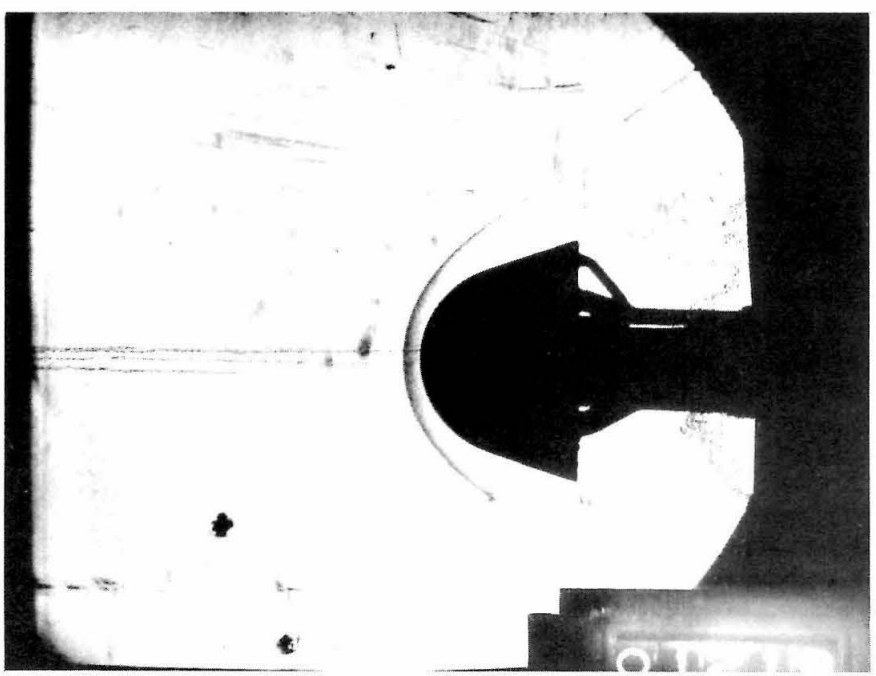

FIG. 11

SCHLIEREN PHOTOGRAPH OF 20° HALF ANGLE CONE

r/R = 0.8, $\alpha = 0^{\circ}$

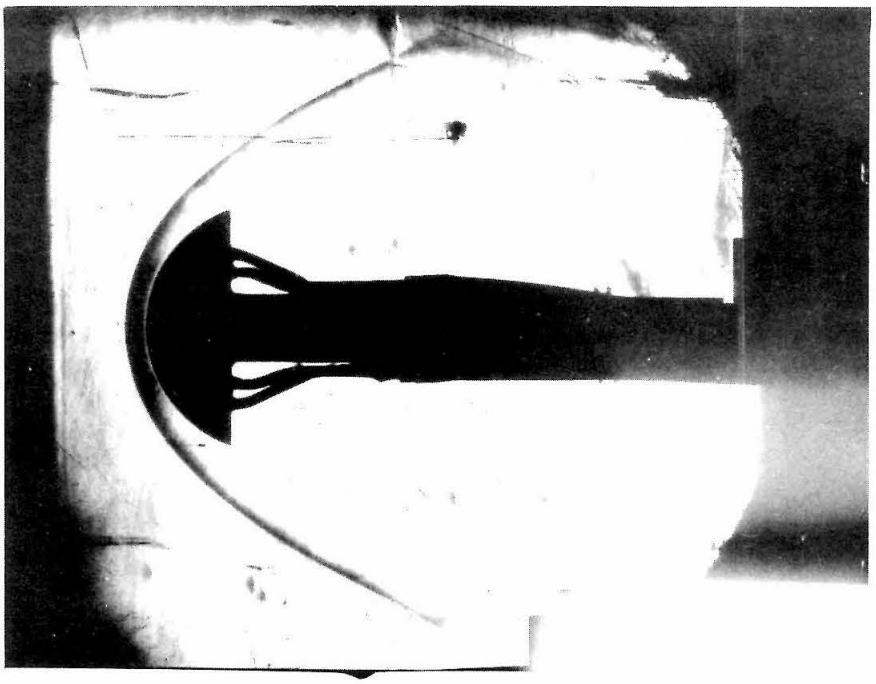

FIG. 12

SCHLIEREN PHOTOGRAPH OF 20° SPHERICAL SECTION

$r/R = 1.064$, $\alpha = 0^\circ$

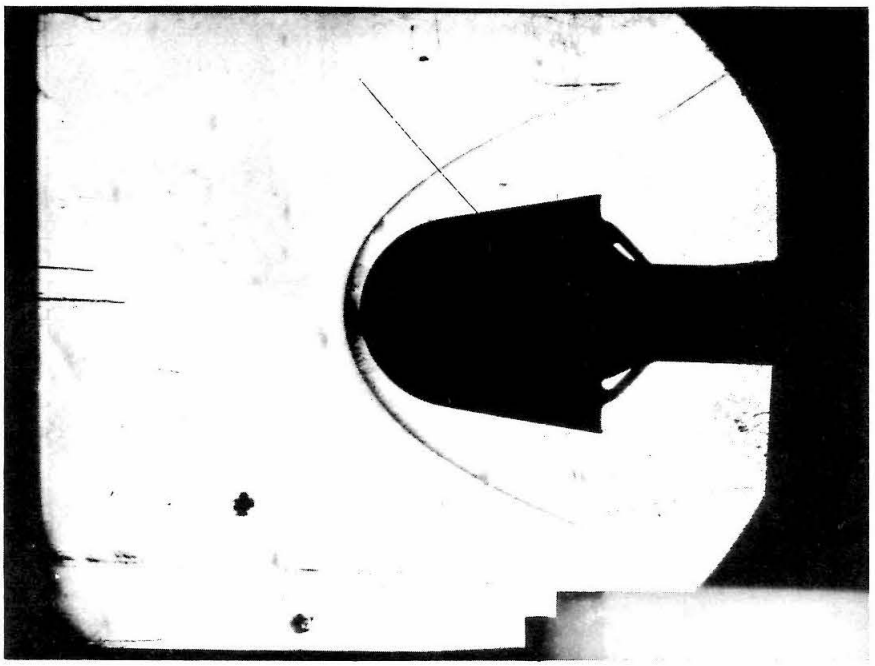

FIG. 13

SCHLIEREN PHOTOGRAPH OF 10° HALF ANGLE CONE

$r/R = 0.8$, $\alpha = 0^\circ$

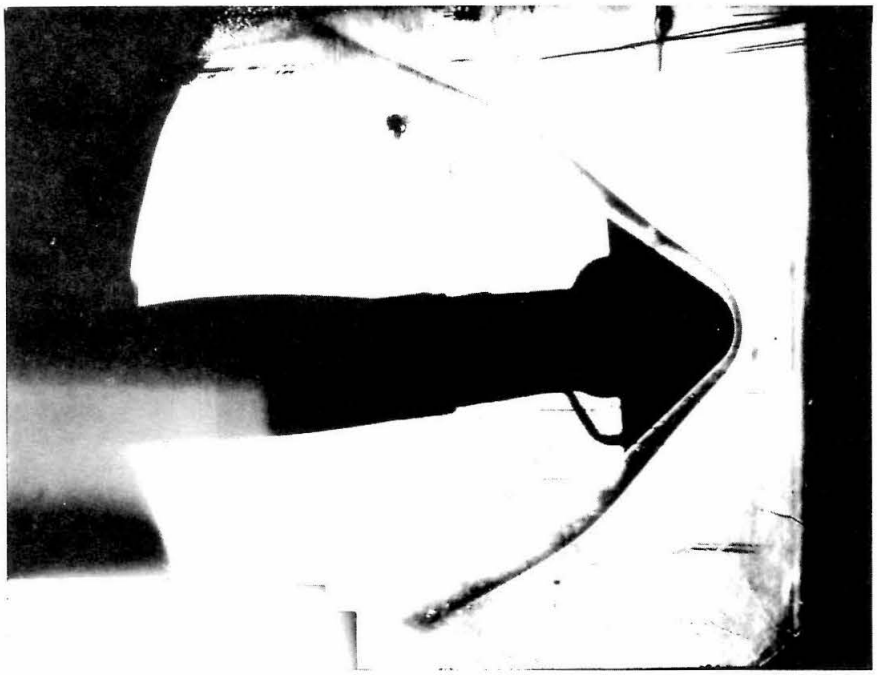

FIG. 14

SCHLIEREN PHOTOGRAPH OF 40° HALF ANGLE CONE

$r/R = 0.4$, $\alpha = 4^{\circ}$

FIG. 15

SCHLIEREN PHOTOGRAPH OF 40° HALF ANGLE CONE

$r/R = 0.4$, $\alpha = 8^{\circ}$

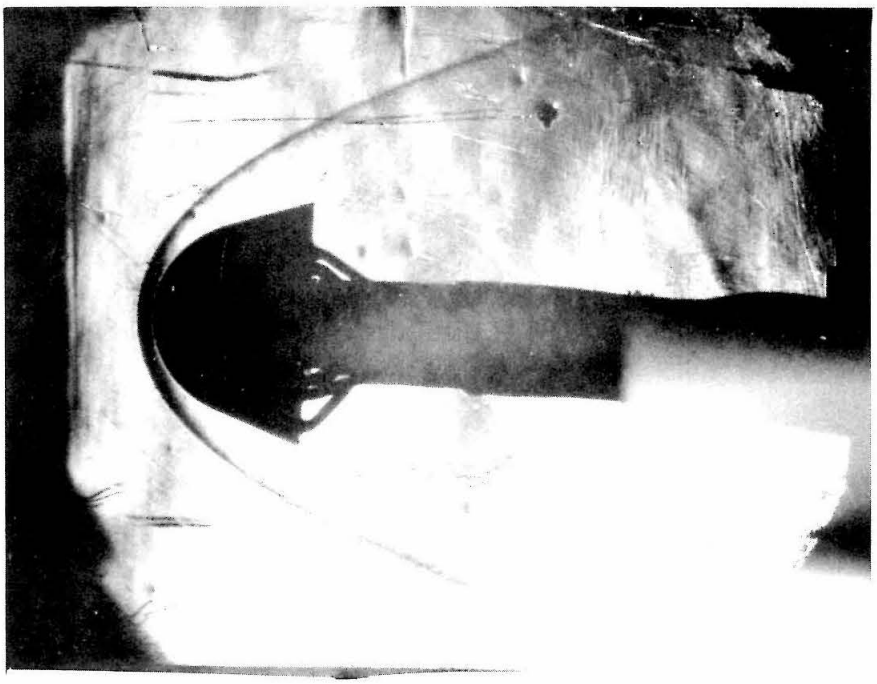

FIG. 16

SCHLIEREN PHOTOGRAPH OF 20° HALF ANGLE CONE

$r/R = 0.8$, $\alpha = 4^{\circ}$

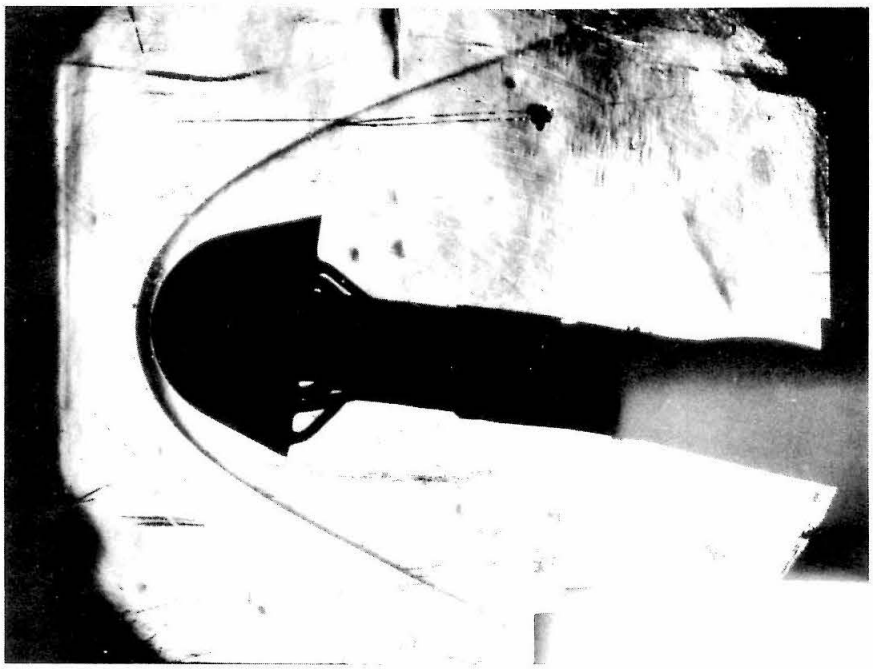

FIG. 17

SCHLIEREN PHOTOGRAPH OF 20° HALF ANGLE CONE

$r/R = 0.8$, $\alpha = 8^{\circ}$

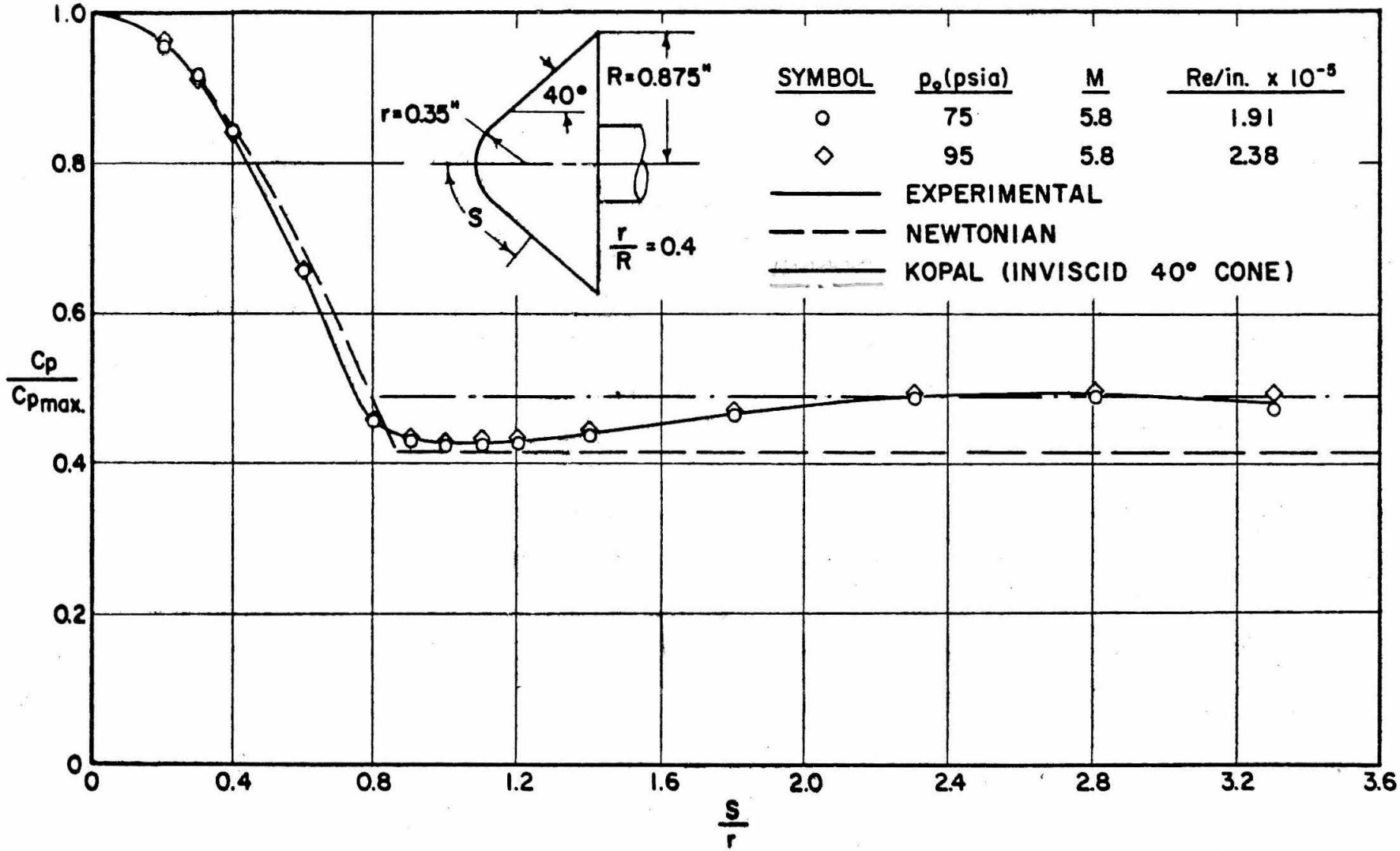

FIG. 18 SURFACE PRESSURE DISTRIBUTION, $\alpha = 0°$

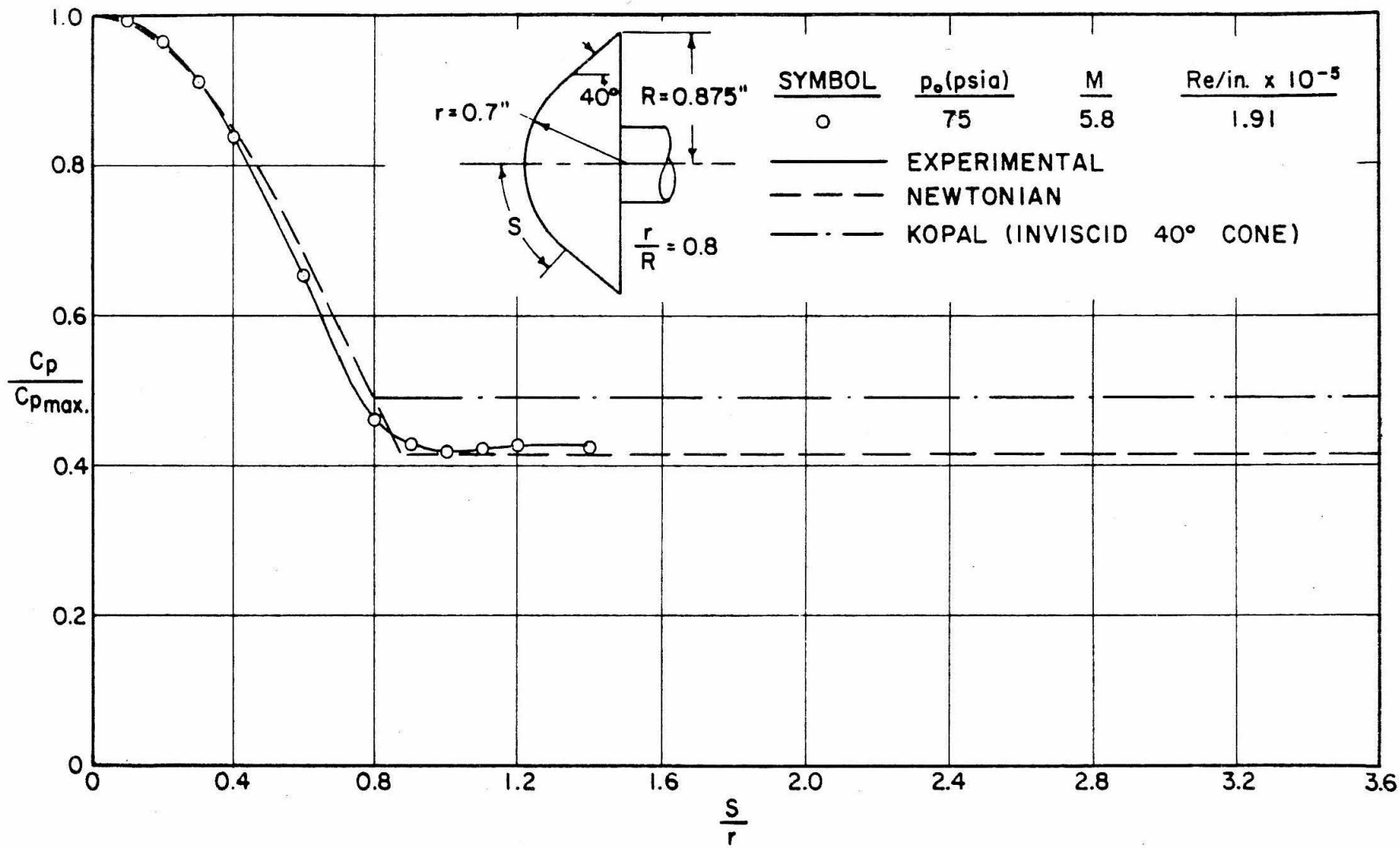

FIG. 19 SURFACE PRESSURE DISTRIBUTION, $\alpha = 0°$

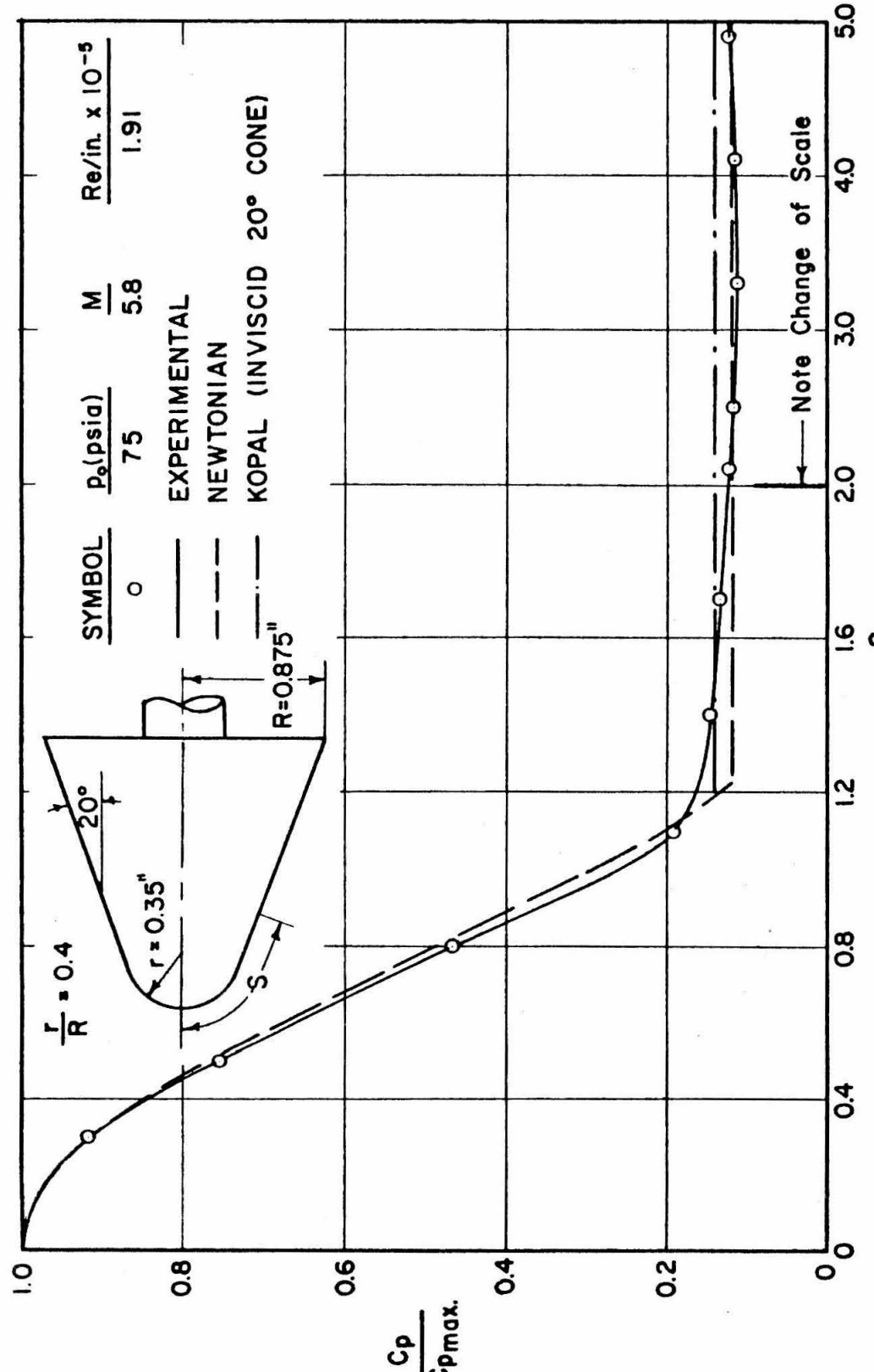

FIG. 20 SURFACE PRESSURE DISTRIBUTION, $\alpha = 0°$

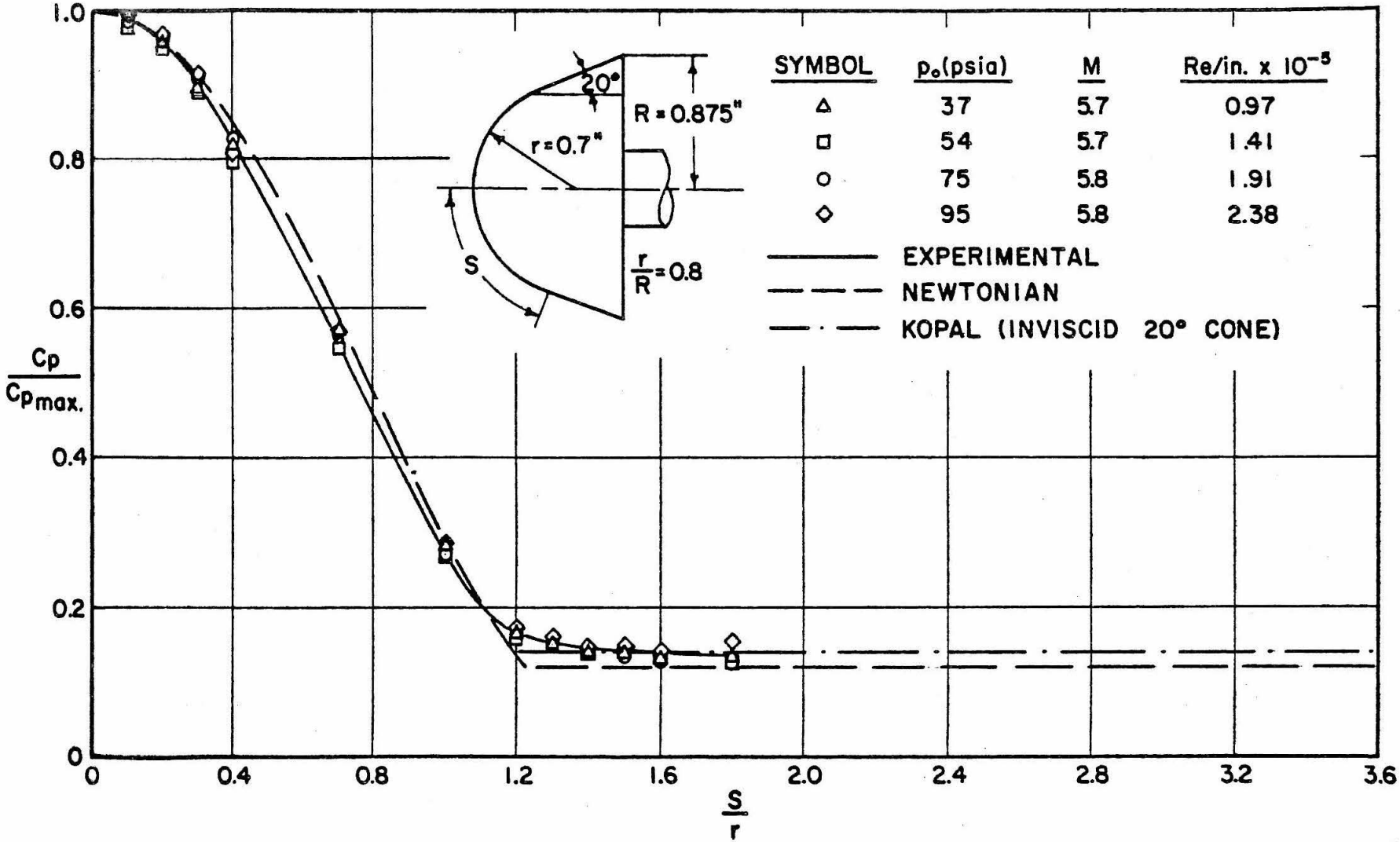

FIG. 21 SURFACE PRESSURE DISTRIBUTION, $\alpha = 0°$

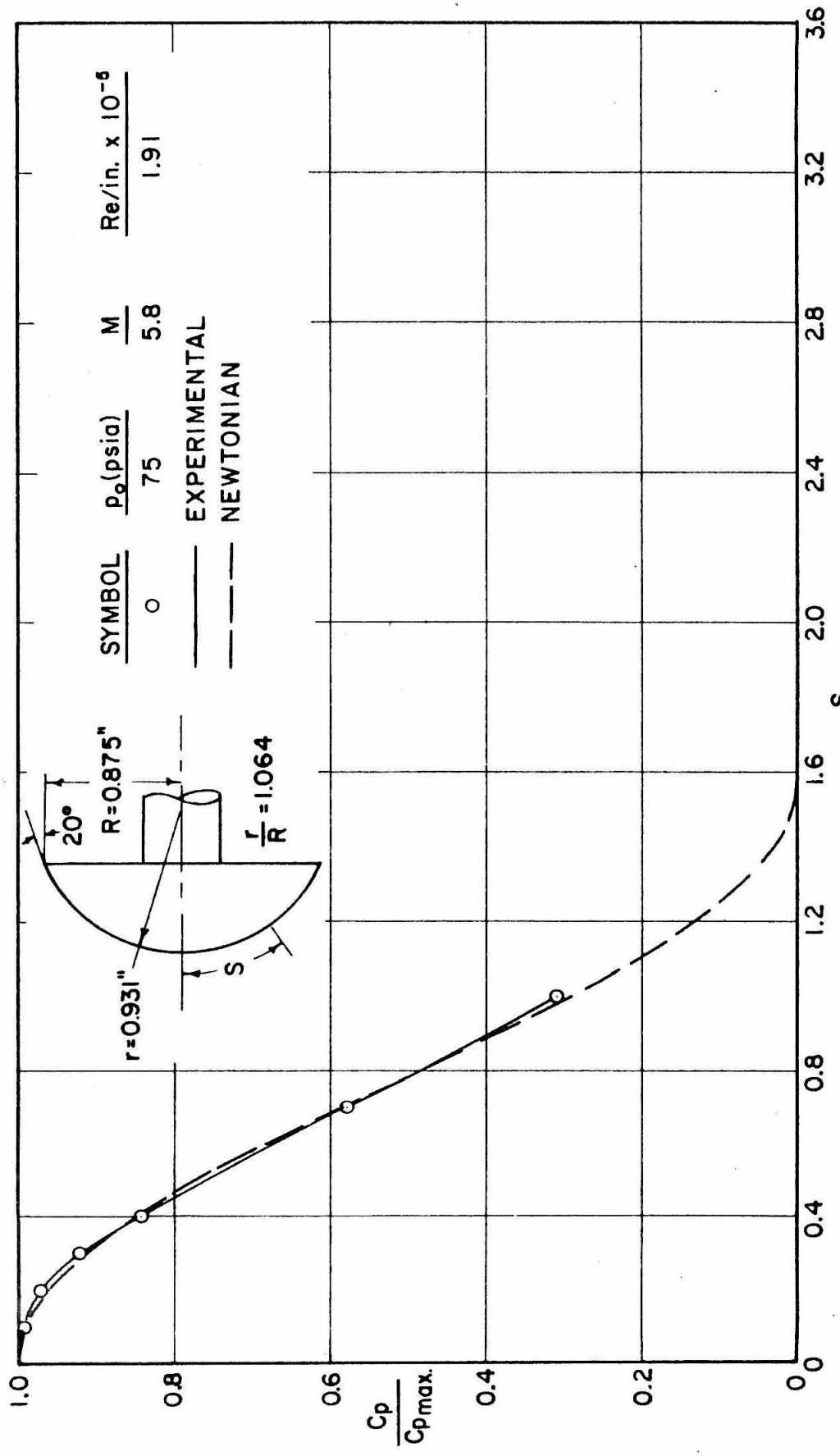

FIG. 22 SURFACE PRESSURE DISTRIBUTION, $\alpha = 0°$

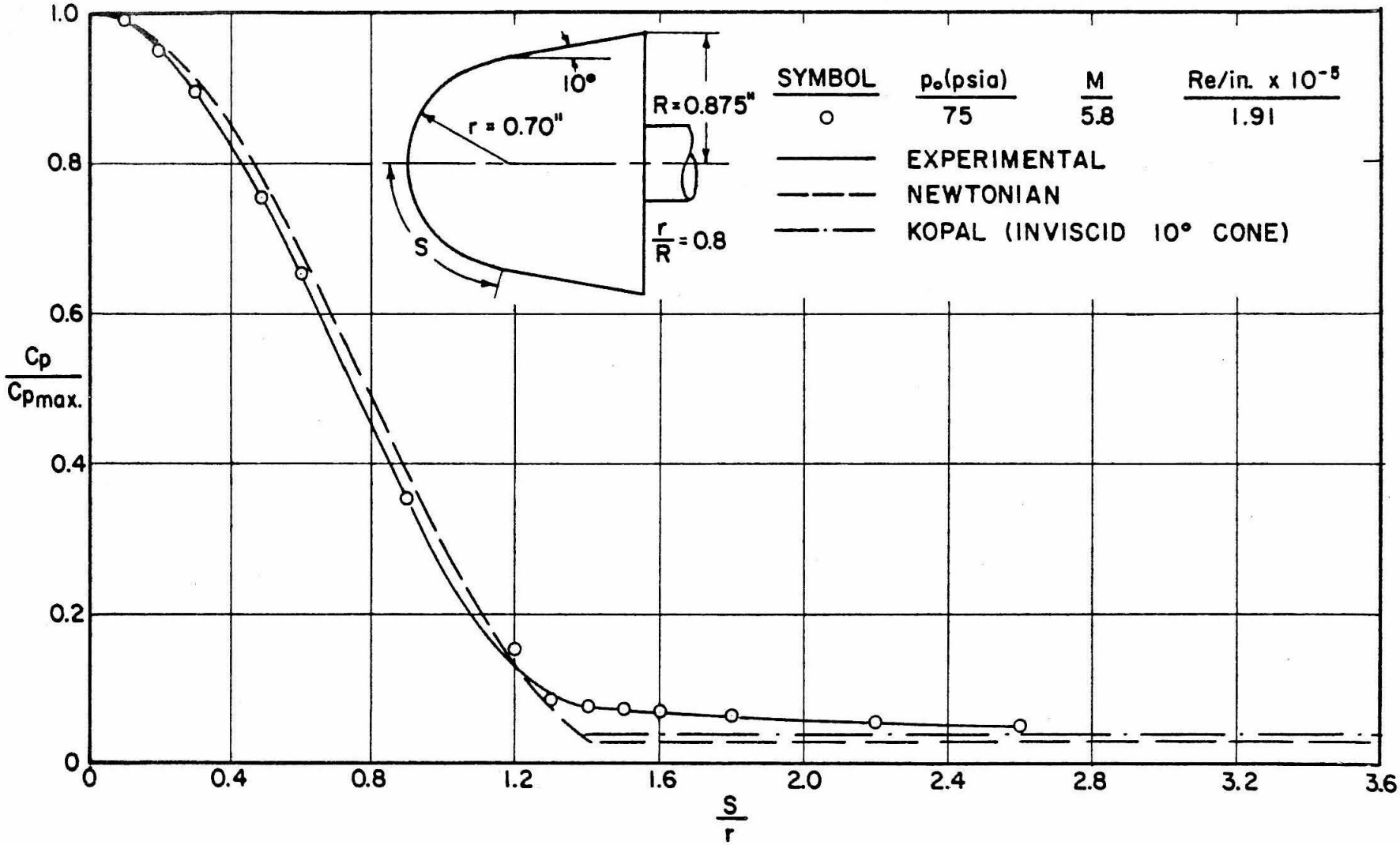

FIG. 23 SURFACE PRESSURE DISTRIBUTION, $\alpha = 0°$

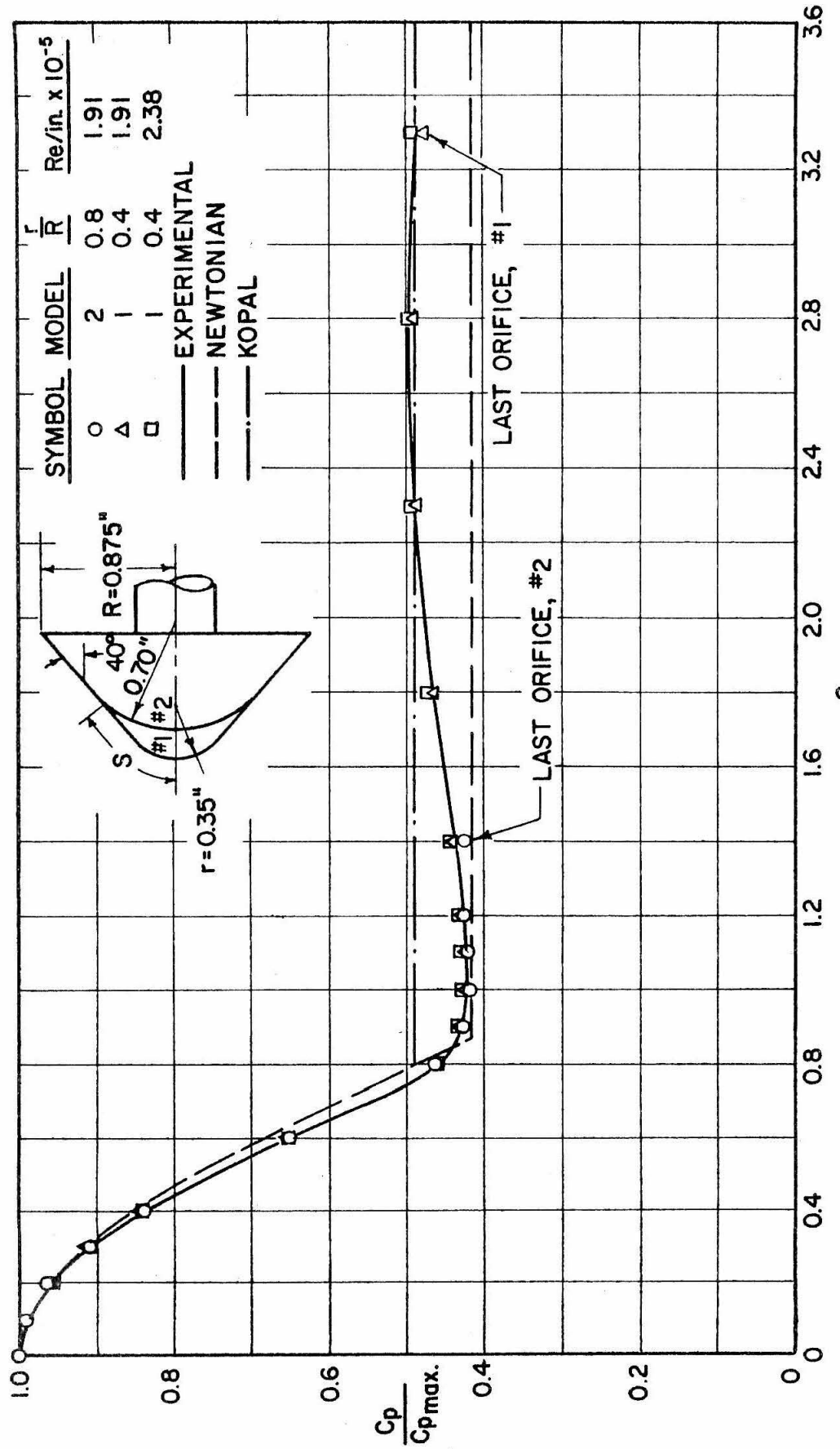

FIG. 24- SURFACE PRESSURE, $\alpha = 0°$

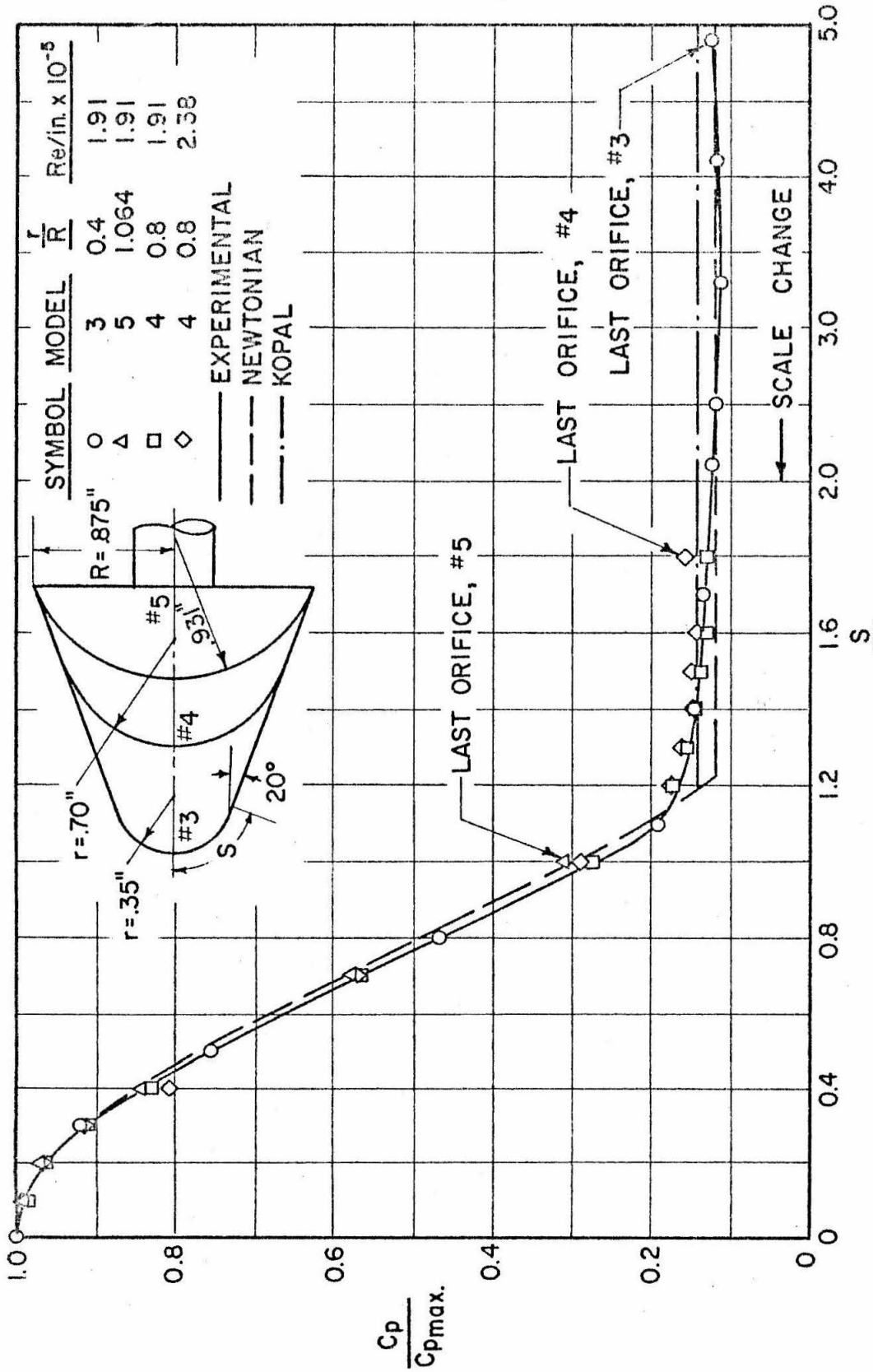

FIG. 25 - SURFACE PRESSURE, $\alpha = 0°$

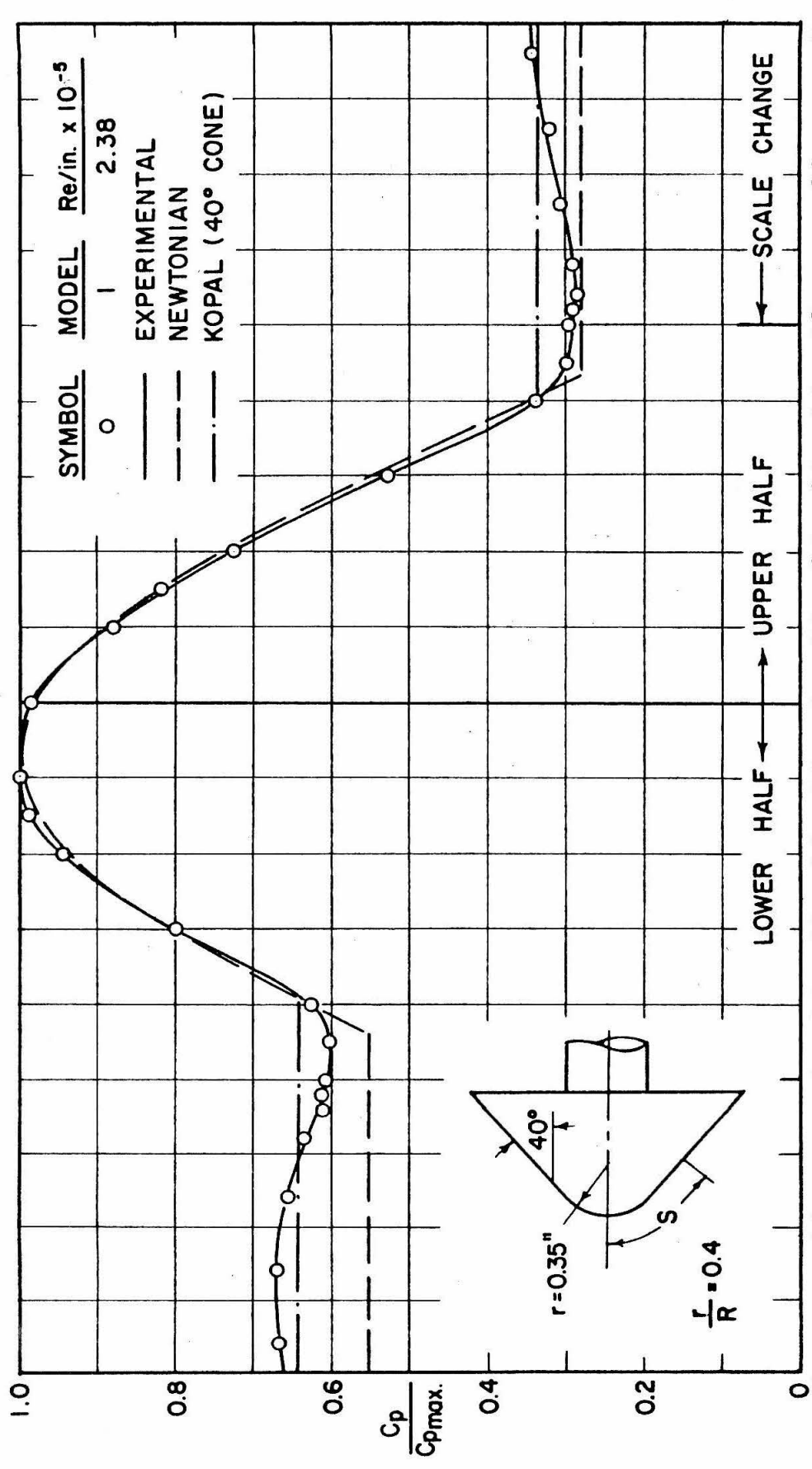

FIG. 26 SURFACE PRESSURE, VERTICAL MERIDIAN PLANE, $\alpha = 8°$

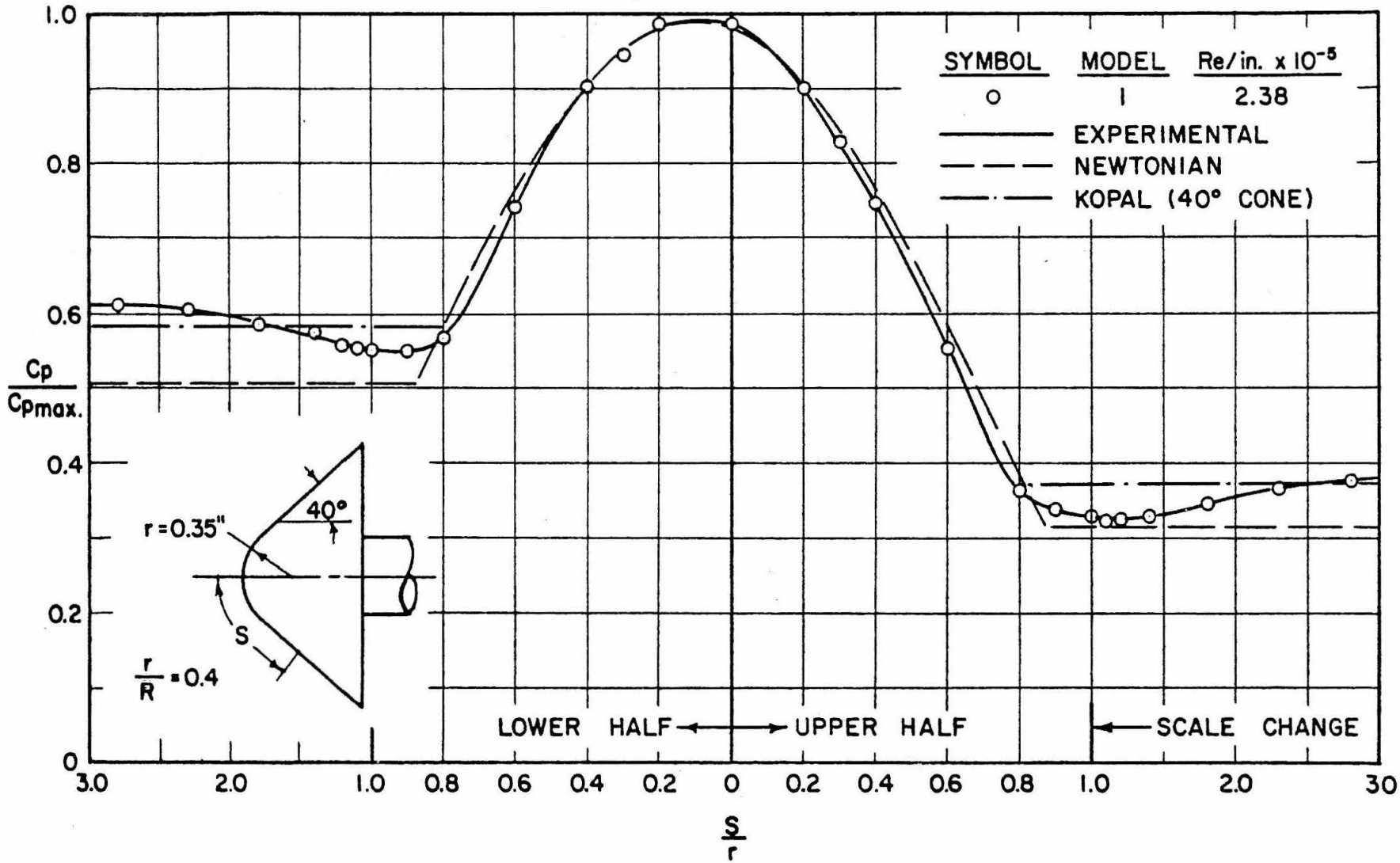

FIG. 27 SURFACE PRESSURE, DIAGONAL MERIDIAN PLANES, $\alpha = 8°$

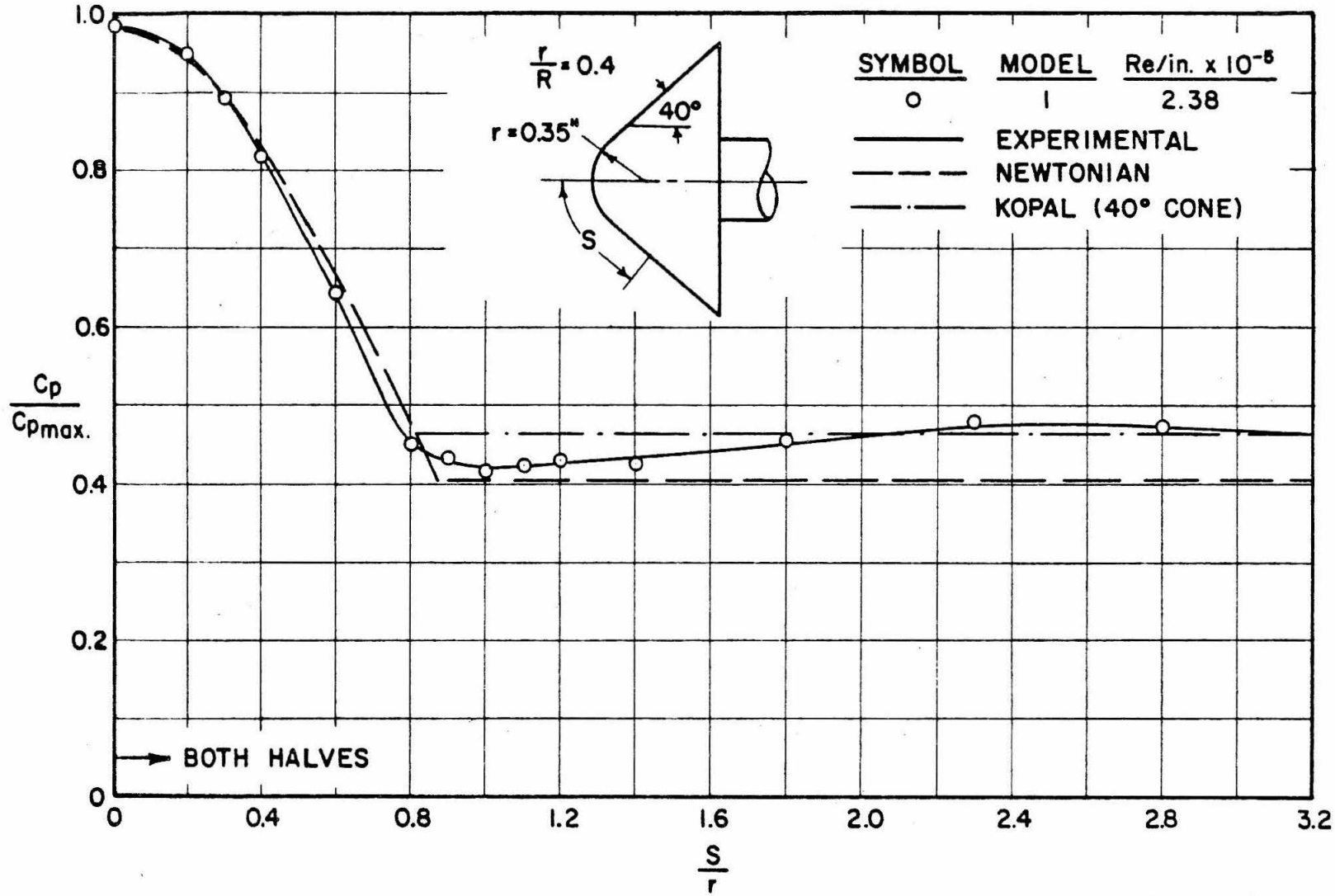

FIG. 28 SURFACE PRESSURE, HORIZONTAL MERIDIAN PLANE, $\alpha = 8°$

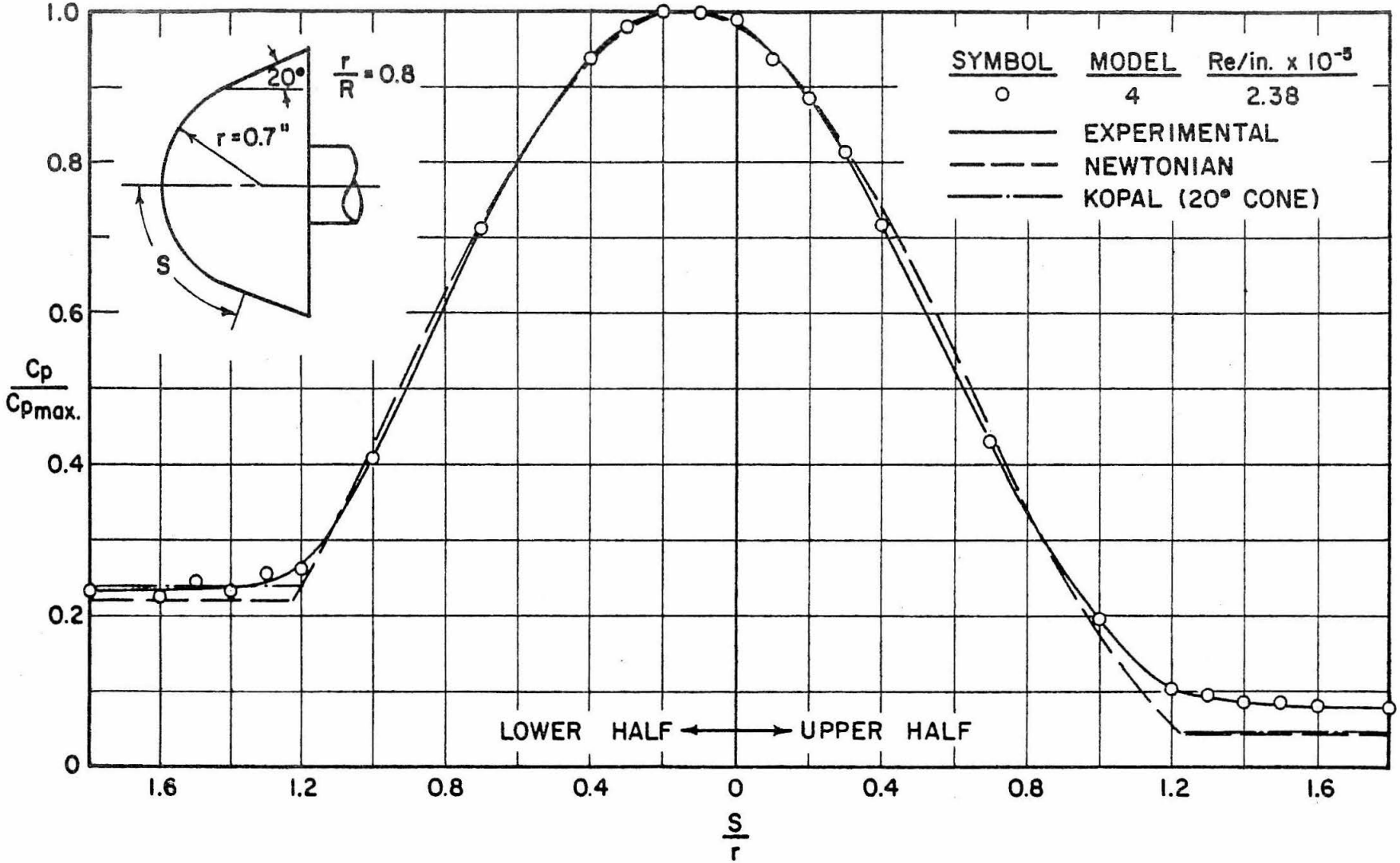

FIG. 29 SURFACE PRESSURE, VERTICAL MERIDIAN PLANE, $\alpha = 8°$

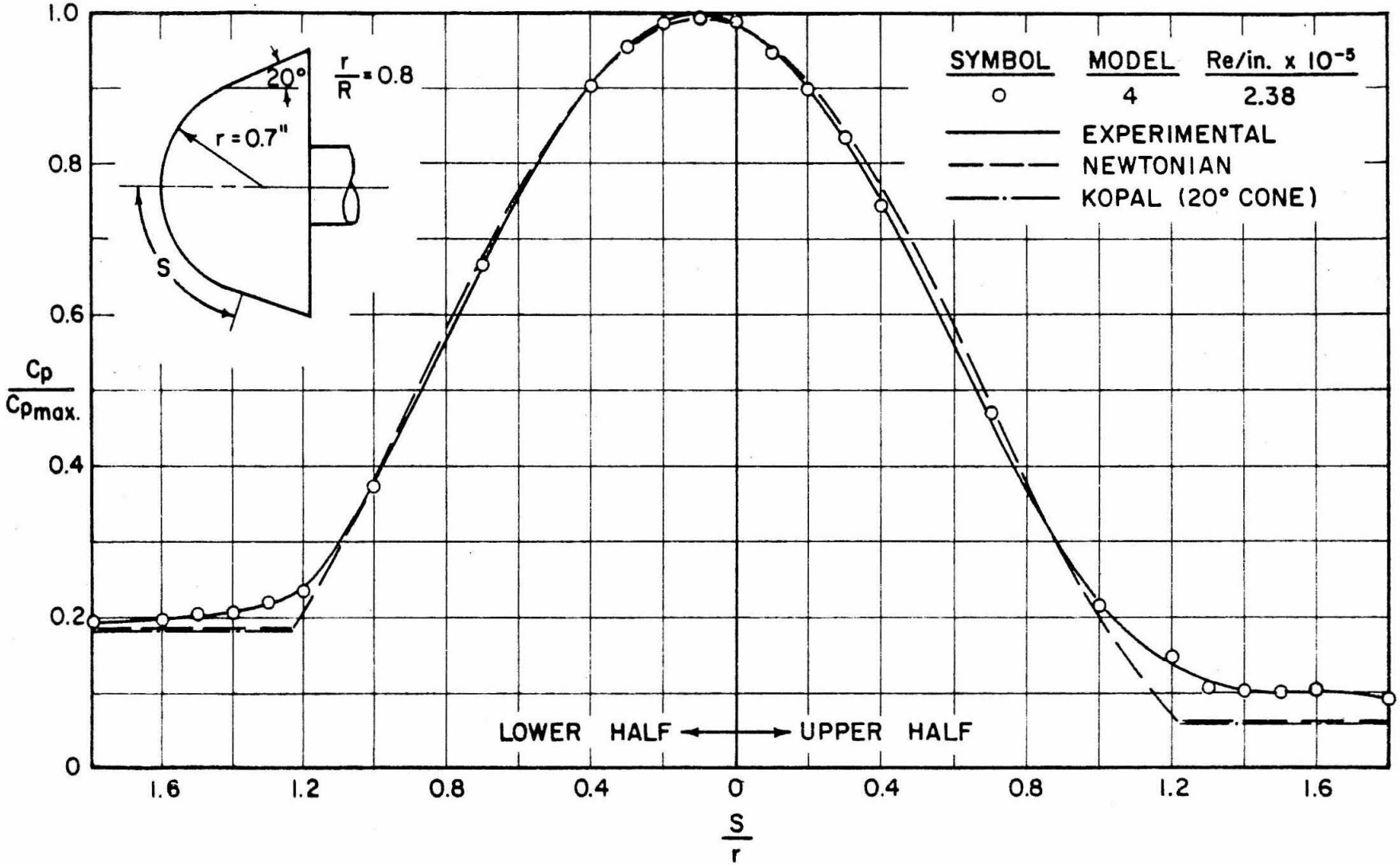

FIG. 30 SURFACE PRESSURE, DIAGONAL MERIDIAN PLANES, $\alpha = 8°$

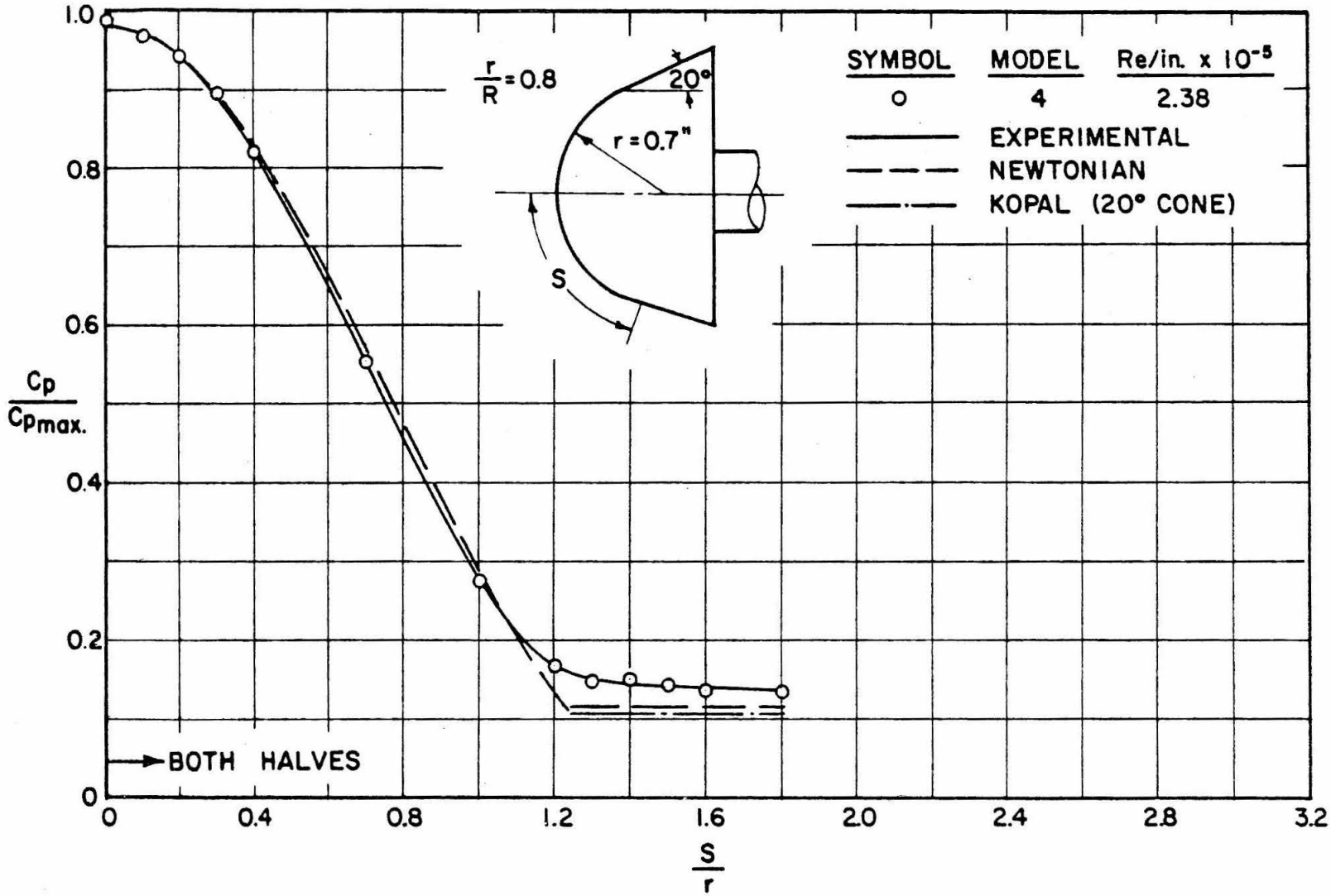

FIG. 31 SURFACE PRESSURE, HORIZONTAL MERIDIAN PLANE, $\alpha = 8°$

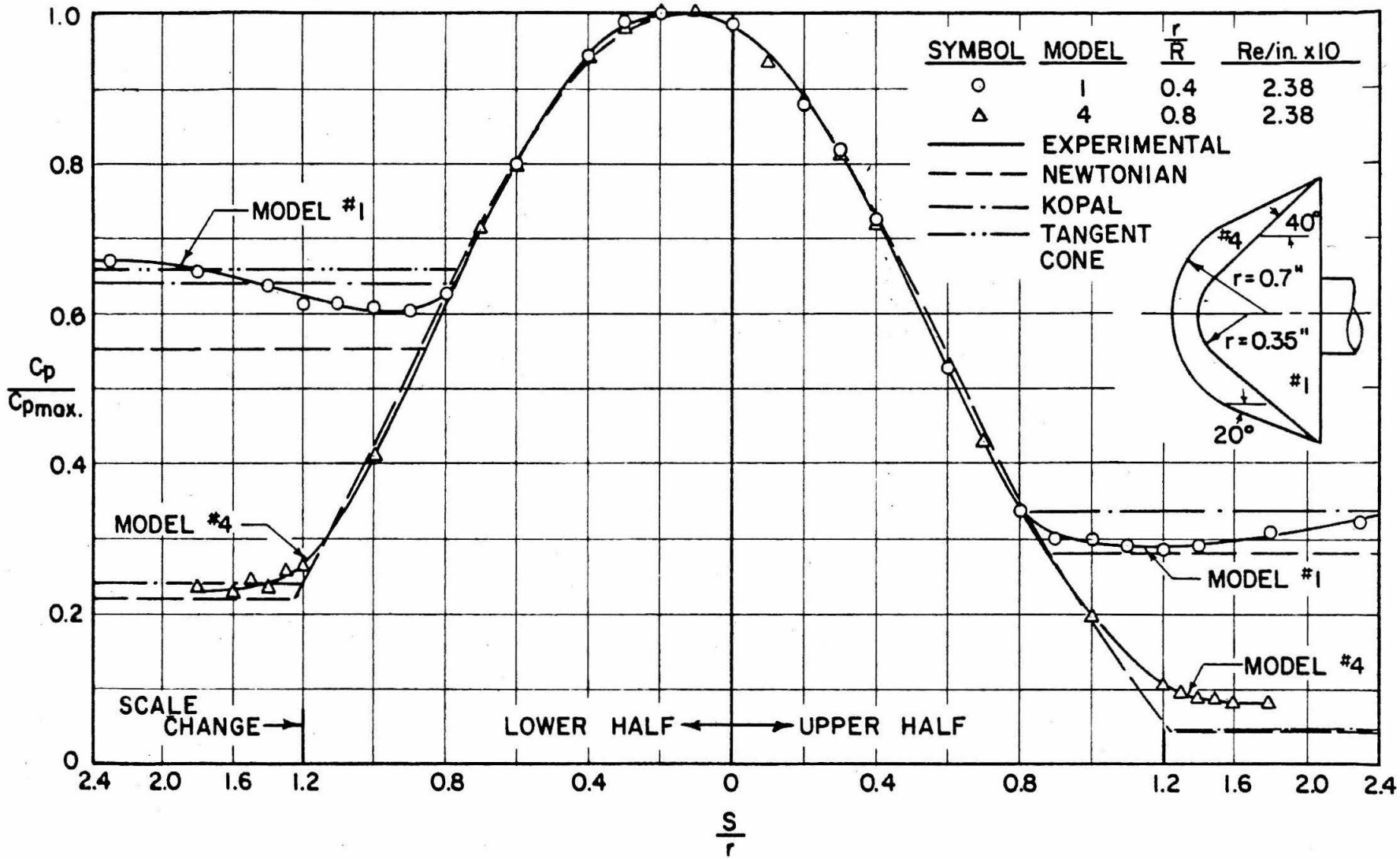

FIG. 32 SURFACE PRESSURE, VERTICAL MERIDIAN PLANE, $\alpha = 8°$

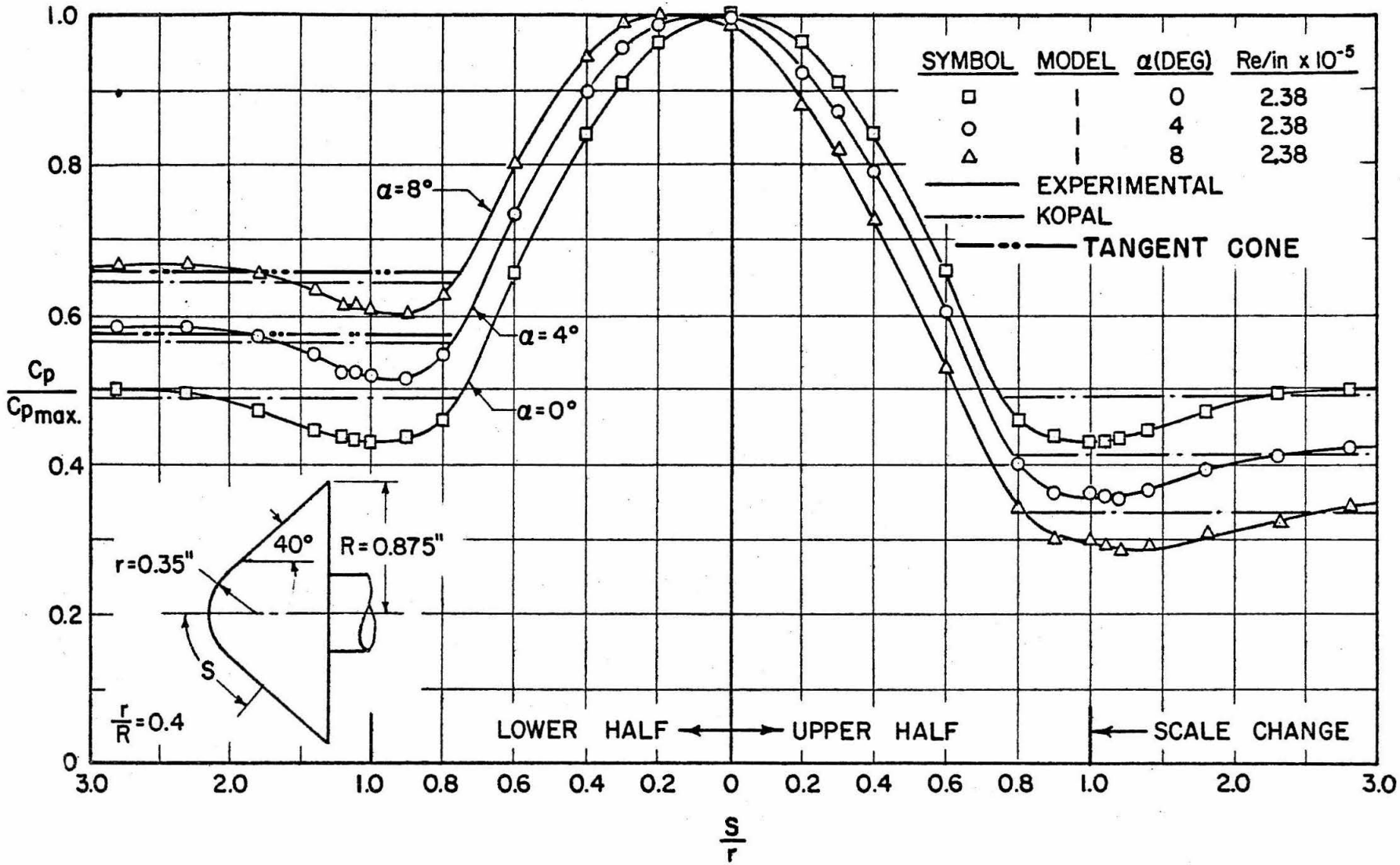

FIG. 33 - SURFACE PRESSURE, VERTICAL MERIDIAN PLANE, $\alpha = 0°, 4°, 8°$

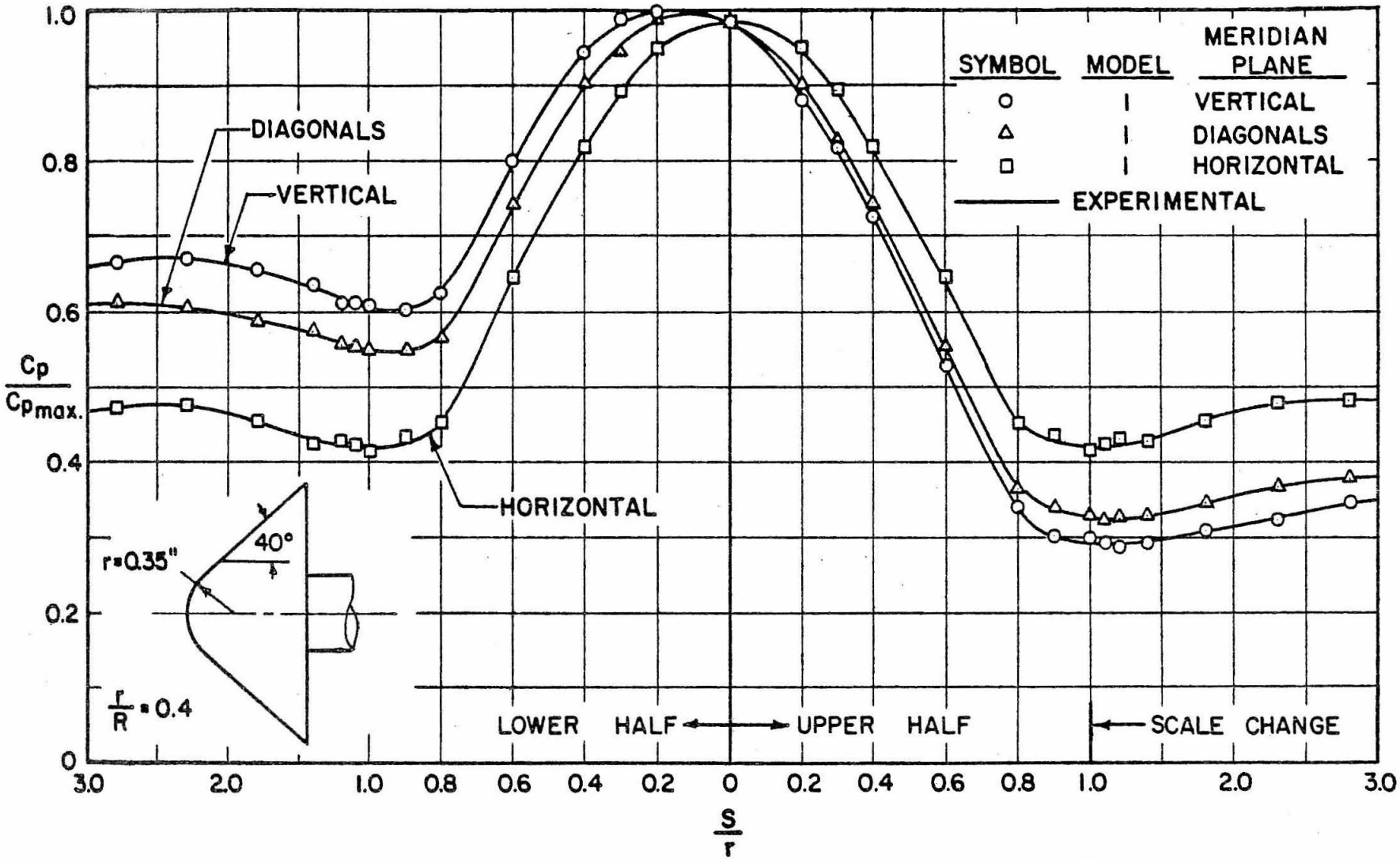

FIG. 34 SURFACE PRESSURE, FOUR MERIDIAN PLANES, $\alpha = 8°$

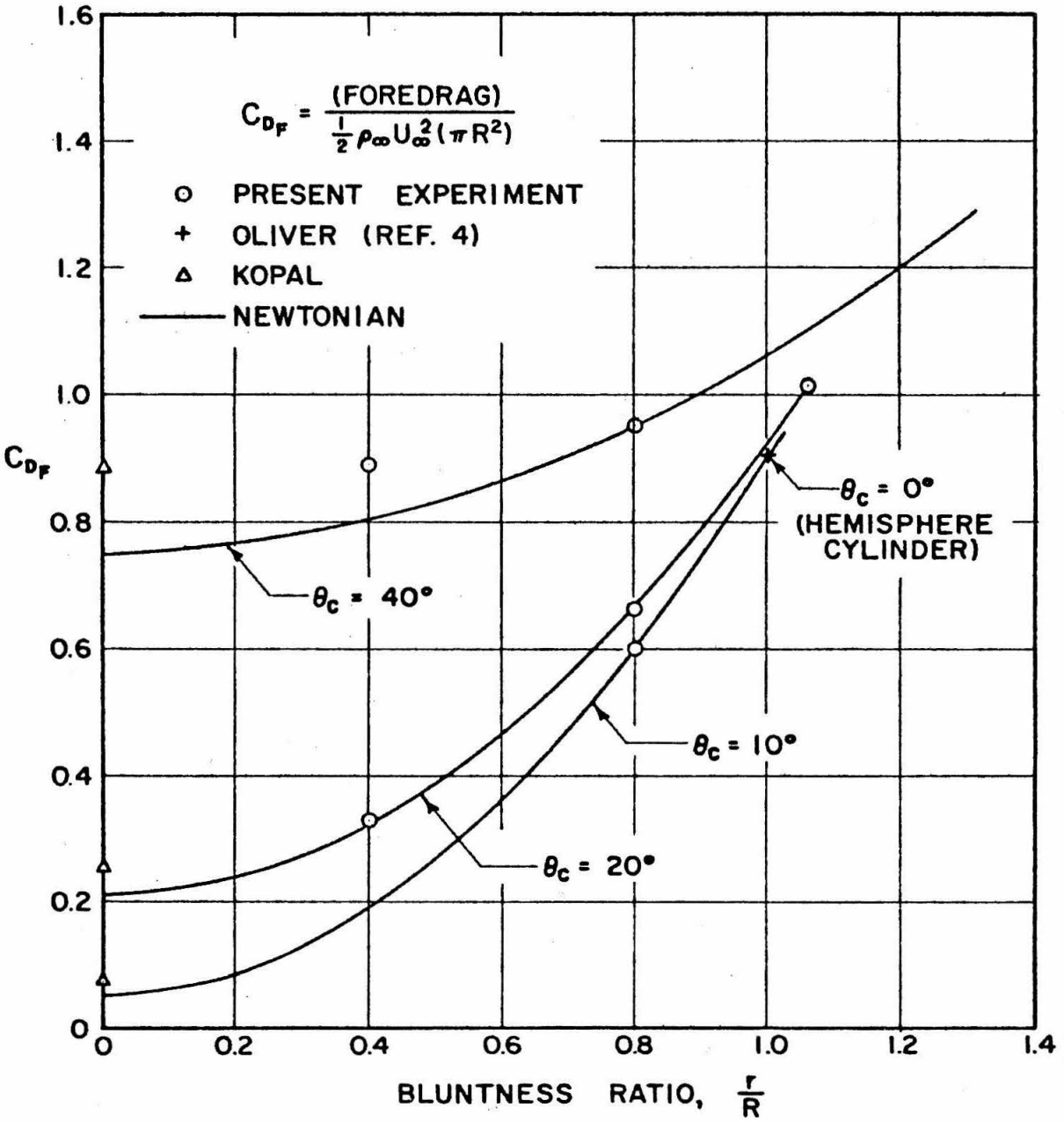

PRESSURE FOREDRAG OF SPHERICAL NOSED CONES AT MACH NUMBER 5.8

FIG. 35

July 1, 1956

GUGGENHEIM AERONAUTICAL LABORATORY
CALIFORNIA INSTITUTE OF TECHNOLOGY

HYPERSONIC RESEARCH PROJECT
Contract No. DA-04-495-Ord-19

DISTRIBUTION LIST

U. S. Government Agencies

Los Angeles Ordnance District
55 South Grand Avenue
Pasadena, California
Attention: Mr. E. L. Stone
2 copies

Western Division
Office of Scientific Research
Hq., Air Research and
Development Command
P. O. Box 2035
Pasadena 2, California
Attention: Dr. Morton Alperin

Office of the Chief of Ordnance
ORDTB - Ballistic Section
The Pentagon
Washington 25, D. C.
Attention: Mr. G. Stetson
2 copies

Office of Ordnance Research
Box CM, Duke Station
Durham, North Carolina
10 copies

Exterior Ballistic Laboratories
Aberdeen Proving Ground
Maryland
Attention: Mr. C. L. Poor

Ballistic Research Laboratories
Aberdeen Proving Ground
Maryland
Attention: Dr. Joseph Sternberg

Commanding General
Headquarters
Air Research and Development
Command
P. O. Box 1395
Baltimore 3, Maryland
Attention: RDTRRF

U. S. Naval Ordnance Laboratory
White Oak
Silver Spring 19, Maryland
Attention: Dr. R. K. Lobb

Commander
Western Development Division
P. O. Box 262
Inglewood, California

Chief of Ordnance
Department of the Army
Washington 25, D. C.
Attention: ORDTB
For Transmittal To
Department of Commerce
Office of Technical Information

Commanding General
Redstone Arsenal
Huntsville, Alabama
Attention: Technical Library

Air Force Armament Center
Air Research and Development Command
Eglin Air Force Base, Florida
Attention: Technical Library

Navy Department
Bureau of Ordnance
Technical Library
Washington 25, D. C.
Attention: Ad-3

Armed Services Technical Information
Agency
Document Service Center
Knott Building
Dayton 2, Ohio
Attention: DSC-SD22
5 copies

Lewis Flight Propulsion Laboratory
National Advisory Committee
for Aeronautics
Cleveland Municipal Airport
Cleveland 11, Ohio
Attention: Dr. A. Silverstein

Lewis Flight Propulsion Laboratory
National Advisory Committee
for Aeronautics
Cleveland Municipal Airport
Cleveland 11, Ohio
Attention: Dr. J. C. Evvard

Ames Aeronautical Laboratory
National Advisory Committee
for Aeronautics
Moffett Field, California
Attention: Mr. H. Julian Allen

Ames Aeronautical Laboratory
National Advisory Committee
for Aeronautics
Moffett Field, California
Attention: Dr. D. Chapman

Ames Aeronautical Laboratory
National Advisory Committee
for Aeronautics
Moffett Field, California
Attention: Dr. A. C. Charters

Ames Aeronautical Laboratory
National Advisory Committee
for Aeronautics
Moffett Field, California
Attention: Mr. A. J. Eggers

Ames Aeronautical Laboratory
National Advisory Committee
for Aeronautics
Moffett Field, California
Attention: Dr. M. K. Rubesin

Holomann Air Force Base
Alamogordo, New Mexico
Attention: Dr. G. Eber

Langley Aeronautical Laboratory
National Advisory Committee
for Aeronautics
Langley Field, Virginia
Attention: Mr. M. Bertram

Langley Aeronautical Laboratory
National Advisory Committee
for Aeronautics
Langley Field, Virginia
Attention: Dr. A. Buseman

Langley Aeronautical Laboratory
National Advisory Committee
for Aeronautics
Langley Field, Virginia
Attention: Mr. C. McLellan

Langley Aeronautical Laboratory
National Advisory Committee
for Aeronautics
Langley Field, Virginia
Attention: Mr. John Stack

National Advisory Committee
for Aeronautics
1512 H Street, N. W.
Washington 25, D. C.
Attention: Dr. H. L. Dryden, Director

National Bureau of Standards
Department of Commerce
Washington 25, D. C.
Attention: Dr. G. B. Schubauer

Naval Ordnance Laboratory
White Oak
Silver Spring, Maryland
Attention: Dr. H. Kurzweg

U. S. Naval Air Missile Test Center
Point Mugu, California
Attention: Mr. J. H. Carrington,
Chief Engineer

U. S. Naval Ordnance Test Station
China Lake
Inyokern, California
Attention: Dr. A. L. Bennett

Commander
Wright Air Development Center
Wright-Patterson Air Force Base
Ohio
Attention: WCLSR

Commander
Wright Air Development Center
Wright-Patterson Air Force Base
Ohio
Attention: WCLSW

Commander
Wright Air Development Center
Wright-Patterson Air Force Base
Ohio
Attention: WCRRD

Commander
Arnold Engineering Development Center
Tullahoma, Tennessee
Attention: AEORL

Director of Research and
Development, DCS/D
Headquarters, USAF
Washington 25, D. C.
Attention: AFDRD-RE

Office of Naval Research
Department of the Navy
Washington 25, D. C.
Attention: Capt. Wm. Fortune

Bureau of Aeronautics
Department of the Navy
Room 2 w 75
Washington 25, D. C.
Attention: Mr. F. A. Louden

Air University Library
Maxwell Air Force Base
Alabama

Commander
U. S. Naval Proving Ground
Dahlgren, Virginia

Technical Information Service
P. O. Box 62
Oak Ridge, Tennessee

Director
Naval Research Laboratory
Washington 25, D. C.

Commanding Officer
Office of Naval Research
Branch Office
Navy, 100
FPO
New York, N. Y.
2 copies

Mechanics Division
Office of Scientific Research
Air Research and
Development Command
P. O. Box 1395
Baltimore, Maryland

Chief of Ordnance
Department of the Army
ORDGU-SE
For Transmittal To
Canadian Joint Staff
Washington, D. C.

Deputy Chief of Staff
for Logistics
U. S. Army
Research and Development
Division
Attention: Research Branch
Washington, D. C.

Commanding General
White Sands Proving Ground
Las Cruces, New Mexico

Universities and Non-Profit Organizations

Brown University
Graduate Division of Applied Mathematics
Providence 12, Rhode Island
Attention: Prof. W. Prager

Brown University
Graduate Division of Applied Mathematics
Providence 12, Rhode Island
Attention: Dr. R. Probstein

University of California at Berkeley
Berkeley, California
Attention: Prof. S. A. Schaaf

University of California at Los Angeles
Department of Engineering
Los Angeles 24, California
Attention: Dr. L. M. K. Boelter

Case Institute of Technology
Cleveland, Ohio
Attention: Dr. G. Kuerti

Catholic University of America
Department of Physics
Washington 17, D. C.
Attention: Prof. K. F. Herzfeld

Cornell Aeronautical Laboratory
Buffalo, New York
Attention: Dr. A. Flax

Cornell Aeronautical Laboratory
Buffalo, New York
Attention: Dr. Ira G. Ross, Director

Cornell University
Graduate School of Aeronautical Engineering
Ithaca, New York
Attention: Dr. A. Kantrowitz

Cornell University
Graduate School of Aeronautical Engineering
Ithaca, New York
Attention: Dr.W. R. Sears

Harvard University
Department of Applied Physics
and Engineering Science
Cambridge 38, Massachusetts
Attention: Dr. A. Bryson

Harvard University
Department of Applied Physics
and Engineering Science
Cambridge 38, Massachusetts
Attention: Dr. H. W. Emmons

The Johns Hopkins University
Applied Physics Laboratory
8621 Georgia Avenue
Silver Spring, Maryland
Attention: Dr. F. N. Frenkiel

The Johns Hopkins University
Department of Aeronautical
Engineering
Baltimore 18, Maryland
Attention: Dr. F. H. Clauser

The Johns Hopkins University
Department of Mechanical
Engineering
Baltimore 18, Maryland
Attention: Dr. S. Corrsin

The Johns Hopkins University
Department of Aeronautical
Engineering
Baltimore 18, Maryland
Attention: Dr. L. Kovasznay

Lehigh University
Physics Department
Bethlehem, Pennsylvania
Attention: Dr. R. Emrich

University of Maryland
Institute of Fluid Dynamics
and Applied Mathematics
College Park, Maryland
Attention: Director

University of Maryland
Department of Aeronautical
Engineering
College Park, Maryland
Attention: Dr. S. F. Shen

Massachusetts Institute of Technology
Cambridge 39, Massachusetts
Attention: Dr. A. H. Shapiro

Massachusetts Institute of Technology
Department of Aeronautical
Engineering
Cambridge 39, Massachusetts
Attention: Dr. G. Stever

Massachusetts Institute of Technology
Department of Aeronautical Engineering
Cambridge 39, Massachusetts
Attention: Prof. M. Finston

Massachusetts Institute of Technology
Department of Aeronautical Engineering
Cambridge 39, Massachusetts
Attention: Prof. J. R. Markham

University of Michigan
Department of Aeronautical Engineering
East Engineering Building
Ann Arbor, Michigan
Attention: Dr. Arnold Kuethe

University of Michigan
Department of Aeronautical Engineering
East Engineering Building
Ann Arbor, Michigan
Attention: Prof. W. C. Nelson

University of Michigan
Department of Physics
Ann Arbor, Michigan
Attention: Dr. O. Laporte

University of Minnesota
Department of Aeronautical Engineering
Minneapolis 14, Minnesota
Attention: Dr. R. Hermann

University of Minnesota
Department of Mechanical Engineering
Division of Thermodynamics
Minneapolis, Minnesota
Attention: Dr. E. R. G. Eckert

National Science Foundation
Washington 25, D. C.
Attention: Dr. R. Seeger

New York University
Department of Aeronautics
University Heights
New York 53, New York
Attention: Dr. J. F. Ludloff

New York University
Institute of Mathematics and Mechanics
45 Fourth Street
New York 53, New York
Attention: Dr. R. W. Courant

North Carolina State College
Department of Engineering
Raleigh, North Carolina
Attention: Prof. R. M. Pinkerton

Ohio State University
Aeronautical Engineering Department
Columbus, Ohio
Attention: Prof. A. Tifford

Ohio State University
Aeronautical Engineering Department
Columbus, Ohio
Attention: Prof. G. L. von Eschen

Pennsylvania State College
Department of Aeronautical
Engineering
State College, Pennsylvania
Attention: Prof. M. Lessen

Polytechnic Institute of Brooklyn
Aerodynamic Laboratory
527 Atlantic Avenue
Freeport, New York
Attention: Dr. A. Ferri

Polytechnic Institute of Brooklyn
Aerodynamic Laboratory
527 Atlantic Avenue
Freeport, New York
Attention: Dr. P. Libby

Princeton University
Forrestal Research Center
Princeton, New Jersey
Attention: Library

Princeton University
Aeronautics Department
Forrestal Research Center
Princeton, New Jersey
Attention: Prof. S. Bogdonoff

Princeton University
Aeronautics Department
Forrestal Research Center
Princeton, New Jersey
Attention: Dr. L. Crocco

Princeton University
Palmer Physical Laboratory
Princeton, New Jersey
Attention: Dr. W. Bleakney

Purdue University
School of Aeronautical Engineering
Lafayette, Indiana
Attention: Librarian

Rensselaer Polytechnic Institute
Aeronautics Department
Troy, New York
Attention: Dr. R. P. Harrington

Rensselaer Polytechnic Institute
Aeronautics Department
Troy, New York
Attention: Dr. T. Y. Li

Rouss Physical Laboratory
University of Virginia
Charlottesville, Virginia
Attention: Dr. J. W. Beams

University of Texas
Defense Research Laboratory
500 East 24th Street
Austin, Texas
Attention: Prof. M. J. Thompson

University of Washington
Department of Aeronautical Engineering
Seattle 5, Washington
Attention: Prof. R. E. Street

University of Wisconsin
Department of Chemistry
Madison, Wisconsin
Attention: Dr. J. O. Hirschfelder

University of Illinois
Department of Aeronautical Engineering
Urbana, Illinois
Attention: Prof. C. H. Fletcher

Institute of the Aeronautical Sciences
2 East 64th Street
New York 21, New York
Attention: Library

Midwest Research Institute
4049 Pennsylvania
Kansas City 11, Missouri
Attention: Mr. M. Goland, Director
for Engineering Sciences

Industrial Companies

Aerophysics Development Corp.
P. O. Box 949
Santa Monica, California
Attention: Librarian

ARO, Inc.
P. O. Box 162
Tullahoma, Tennessee
Attention: Mr. R. Smelt

ARO, Inc.
Tullahoma, Tennessee
Attention: Dr. B. Goethert

AVCO Manufacturing Corp.
2385 Revere Beach Parkway
Everett 49, Massachusetts

Bell Aircraft Corp.
P. O. Box 1
Buffalo 5, New York
Attention: Mr. R. J. Woods

Boeing Airplane Company
P. O. Box 3107
Seattle 14, Washington
Attention: Mr. G. Snyder

Chance Vought Aircraft, Inc.
P. O. Box 5907
Dallas, Texas
Attention: Mr. J. R. Clark

CONVAIR
Division of General Dynamics Corp.
San Diego 12, California
Attention: Mr. C. Bossart

CONVAIR
Division of General Dynamics Corp.
San Diego 12, California
Attention: Mr. W. H. Dorrance
Dept. 1-16

CONVAIR
Division of General Dynamics Corp.
Fort Worth 1, Texas
Attention: Mr. R. H. Widmer

Douglas Aircraft Company
Santa Monica, California
Attention: Mr. H. Luskin

General Electric Company
Research Laboratory
Schenectady, New York
Attention: Dr. H. T. Nagamatsu

General Electric Company
Campbell Avenue Plant
Schenectady, New York
Attention: Mr. G. Metcalf

The Glenn L. Martin Company
Baltimore 3, Maryland
Attention: Mr. G. S. Trimble, Jr.

Grumman Aircraft Engineering Corp.
Bethpage, New York
Attention: Mr. C. Tilgner, Jr.

Hughes Aircraft Company
Culver City, California
Attention: Dr. A. E. Puckett

Lockheed Aircraft Corp.
Missiles Division
Van Nuys, California
Attention: Library

Marquhardt Aircraft Company
P. O. Box 2013 - South Annex
Van Nuys, California
Attention: Dr. P. D. Arthur

McDonnell Aircraft Corp.
Lambert-St. Louis Municipal Airport
P. O. Box 516
St. Louis 3, Missouri
Attention: Mr. K. Perkins

North American Aviation, Inc.
Aeronautical Laboratory
Downey, California
Attention: Dr. E. R. Van Driest

Northrop Aircraft, Inc.
1001 East Broadway
Hawthorne, California
Attention: Mr. E. Schmued

Ramo-Wooldridge Corporation
409 East Manchester Blvd.
Inglewood, California
Attention: Dr. Louis G. Dunn

The RAND Corporation
1700 Main Street
Santa Monica, California
Attention: Librarian

The RAND Corporation
1700 Main Street
Santa Monica, California
Attention: Mr. E. P. Williams

Republic Aviation Corporation
Conklin Street
Farmingdale, L. I., New York
Attention: Dr. W. J. O'Donnell

United Aircraft Corp.
East Hartford, Connecticut
Attention: Mr. J. G. Lee

Internal

Jet Propulsion Laboratory
4800 Oak Grove Drive
Pasadena 2, California
Attention: Reports Group

Dr. Peter P. Wegener
Jet Propulsion Laboratory

Goddard Professor
Jet Propulsion Center
California Institute of Technology

Aeronautics Library
Hypersonic Staff and Research Workers (22)
Hypersonic Files (3)